2000

Applications and progress in modeling of one and two dimensional photonic crystals

Casey Martin Clark
University of Dayton

APPLICATIONS AND PROGRESS IN MODELING OF ONE AND TWO DIMENSIONAL PHOTONIC CRYSTALS

Thesis

Submitted to

The School of Engineering of the

UNIVERSITY OF DAYTON

In Partial Fulfillment of the Requirements for

The Degree

Master of Science in Electro-Optics

By

Casey Martin Clark

UNIVERSITY OF DAYTON

Dayton, Ohio

December 2000

APPLICATIONS AND PROGRESS IN MODELING OF ONE AND TWO DIMENSIONAL PHOTONIC CRYSTALS

APPROVED BY:

[redacted]

Peter E. Powers, Ph. D.
Assistant Professor, Physics
& Electro-Optics
Committee Chairman

[redacted]

Sean M. Kirkpatrick, Ph. D.
Senior Research Scientist, SAIC
Committee Member

[redacted]

Joseph W. Haus, Ph. D.
Director, Electro-Optics
Committee Member

[redacted]

Donald L. Moon, Ph. D.
Associate Dean
Graduate Engineering Programs
& Research
School of Engineering

[redacted]

Blake Cherrington, Ph. D., P. E.
Dean, School of Engineering

ABSTRACT

APPLICATIONS AND PROGRESS IN MODELING OF ONE AND TWO DIMENSIONAL PHOTONIC CRYSTALS

Name: Clark, Casey Martin
University of Dayton, 2000

Advisor: Dr. Sean Kirkpatrick

Photonic crystals operating in the optical wavelength region of the spectrum have been examined extensively in the recent past due to their promise in optical processing applications. Several methods of fabrication exist for these structures, however, holographic techniques and specifically holographic two-photon induced photopolymerization (H-TPIP) shows promise as an economical and widely applicable technique for fabricating multidimensional photonic crystals. Incorporation of optically active materials such as liquid crystal, nonlinear materials, and gain media into photonic crystal structures can produce passive and active, filters and switches, and novel source devices. The successful construction of one and two-dimensional photonic crystals, operating in the visible to near infrared wavelength region, along with the incorporation of linear and nonlinear materials inside these structures is reported. Experimental examination of these structures is presented in this work, as well as a comparison of fabrication techniques. Progress in theoretical response is also reported.

ACKNOWLEDGEMENTS

Throughout my life my family has been incredibly supportive and has always let me find my way. Without my mother and father, my sister Carin and my brother David, who always inspired me to keep going, I may have never faced this challenge and certainly not have accomplished this. The past several months were made so much easier as a result of Marney's undying love and support, without her I probably would have gone insane. For practically my entire life Tyler and Kevin have challenged me and inspired me to become the biggest nerd that I could, I want to thank them and all of my other friends who helped my to get where I am now. Finally, I would like to thank my advisor Sean, who inspired me and gave me more opportunity and support than I could have ever asked for.

TABLE OF CONTENTS

LIST OF FIGURE

INTRODUCTION

Photonic crystals have been studied extensively in the recent past as a result of their unique properties regarding the control of light propagation. These structures can exhibit a photonic band gap in which no wavelength falling inside the gap will propagate [1-15]. This feature offers the ability to construct narrow band filters, laser cavities, and waveguides. In addition to these applications photonic crystal structures offer the unique ability of providing a host for various optically active materials for the purpose of creating a dynamic system.

Photonic crystals consist of a low loss periodic dielectric material with the periodicity of the dielectric constants in one, two, or three dimensions. The focus of this work will be on one-dimensional and two-dimensional photonic crystal structures. The distributed Bragg reflector and an ordered array of channels in a dielectric or semiconductor substrate are examples of one and two-dimensional photonic crystals, respectively. Due to the periodicity of these materials the Bloch wave analysis is used to solve the wave equations. Solutions to the wave equations are the Bloch wave functions, which, according to the Bloch theorem, are periodic with the same periodicity as the medium in question. Several methods have been devised to calculate the frequency band structure for these

types of materials including an approach based on the electromagnetic variational theorem and a generalized eigenvalue solution [1,4-15]. These methods have been shown to be consistent with experiment [1-8], but are limited by factors such as the assumption that the material extends to infinity and the fact that these solutions can not take into account any dynamics or defects of the system. To overcome these limitations a Split-Step Beam Propagation Method (BPM) approach was designed to model these systems.

Photonic crystal structures, which are functional in the range of optical radiation, must have features with dimensions on the order of the wavelength of light. Several techniques exist for the manufacture of these types of structures including, micro-machining, photolithography, holographic one-photon induced photopolymerization, holographic two-photon induced photopolymerization (H-TPIP), and bias sputtering [31-36]. Holography and specifically holographic two-photon induced photopolymerization has recently been examined as a viable technique for micro and nano-fabrication [31,37]. In this method the interference of coherent ultrafast pulses causes high intensity regions to exist at the recording medium in the form of sinusoidal patterns, planes, columns, or isolated regions in a three-dimensional matrix. Grating structures along with multidimensional photonic crystals can be constructed with this process. In addition to these methods, a glass drawing technique has been devised at the Naval Research Laboratories (NRL) in Washington D.C. which produces two dimensional photonic crystals with air channels in a glass substrate [42,43]. Construction of one-

dimensional and two-dimensional photonic crystals via H-TPIP and the glass drawing method will be examined in the following.

Advancements in communication and the advent of optical computing will necessitate the ability to switch information very rapidly. It is of interest to examine the possibility of a dynamic system in which the band structure of a photonic crystal changes with some arbitrary input, therefore providing a dynamic filter or optical switch. An approach to dynamic photonic band gap structures lies in the use of liquid crystal in a periodic matrix such as a polymer dispersed liquid crystal (PDLC) [16], the planes of a photopolymerized one-dimensional photonic crystal, or the channels of a two dimensional photonic crystal. Liquid crystal (LC) has been incorporated into many devices including liquid crystal displays (LCD) and optical switches [45,46]. In these structures the liquid crystal can be switched in order to index match to the surrounding material or index mismatch to the surrounding material, thus diffracting radiation or producing a photonic band gap. Waveguiding can also occur in the channels of a two-dimensional photonic crystal by incorporating a material with a higher refractive index than that of the matrix material. It is believed that by including LC into the channels of a two-dimensional photonic structure one can induce or inhibit waveguiding. It is also believed that intensity dependent filters can be constructed using a photonic crystal by incorporating into the structure a material with a large nonlinear index of refraction [16,61]. When the appropriate field is applied to the structure the index of the nonlinear material can be altered to produce a band gap for a particular wavelength. Incorporating a nonlinear material, exhibiting a thermal nonlinearity,

into the channels of a NCG sample has shown dynamic behavior of the photonic band gap of a two-dimensional photonic crystal [61].

Low-lying manifolds of rare earth ions have transitions in the mid infrared and, provided there is limited multiphonon quenching, have the potential to act as mid infrared sources of radiation due to their ground state splitting. Doping rare earth ions, such as Er^{+3} and Tb^{+3}, into a low phonon host eliminates multiphonon quenching and enhances radiative emission [49-54]. Hosts such as $GdCl_3$ and $LaCl_3$ have a low phonon density of states and readily incorporate these materials into their lattice structures but have the disadvantage of being hygroscopic. Growth of these materials inside a two-dimensional photonic crystal can overcome this hygroscopic nature of these materials by providing isolation from the environment. It is also believed that some of the IR emission and absorption transitions of the rare earth low phonon crystals will be affected by growing these materials inside these structures [55,56].

This thesis presents the results of the successful construction of one and two-dimensional photonic crystals and the incorporation of linear and nonlinear materials into these structures. Chapter 1 deals with the analysis of these materials from an analytical and numerical perspective. In chapter 2 the methods for the construction of one and two-dimensional photonic crystal structures and the results of these methods are discussed. The incorporation of liquid crystal and nonlinear materials into the photonic band gap materials is presented in chapter 3. A discussion of rare earth doped low phonon laser and detector crystals and the growth process inside the channels of a two-dimensional photonic crystal are

presented in chapter 4. Chapter 5 discusses conclusions and proposed directions for future work.

CHAPTER 1

Photonic Crystals

Photonic crystals consist of a low loss periodic dielectric material with the periodicity of the dielectric constants in one, two, or three dimensions. A photonic crystal can be employed to control the propagation of light in specific directions through the material and it is possible to design a photonic crystal with a photonic band gap, preventing light of a particular frequency range from propagating. If a photonic crystal is constructed such that light of a specific frequency is reflected, regardless of the polarization and propagation direction, the material is said to have a complete band gap [1]. The focus of this work will be on one-dimensional and two-dimensional photonic crystal structures, which do not exhibit a complete band gap due to the fact that the periodicity does not exist in three dimensions. Light, which does not propagate through the material, is reflected at Bragg angles similar to reflections from the atoms of a crystal. Unlike

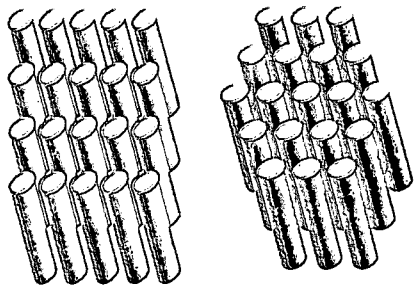

Figure 1.1 Square and Triangular Lattice

the spacing of lattice points in a crystal a photonic crystal has periods on the order of a wavelength of optical radiation. These structures and their applications have been examined extensively in the recent past [1,2,3]. While the transmission through a one-dimensional photonic crystal is wavelength dependent, at normal incidence it is not polarization dependent. The study of one-dimensional photonic crystals will be limited to this case. A lattice consisting of an ordered array of cylindrical channels inside a homogenous dielectric medium is an example of a two-dimensional photonic crystal. Lattice structures for the channels, illustrated in figure 1.1, can be in either a square matrix or a triangular matrix. Propagation in the two-dimensional photonic crystals will be limited to the plane normal to the axis of the cylinders. A triangular lattice has an advantage over the square lattice due to the fact that the polarization dependent band gaps can overlap. Understanding these properties regarding the frequency dependence of the transmission is of primary interest. Several methods have been devised to calculate the frequency band structure for these types of materials, including an approach based on the electromagnetic variation theorem and an eigenvalue solution [1,4-15]. These methods have been shown to be consistent with experiment but are limited by factors such as difficulty in taking into account any dynamics of the system and the assumption that the materials in question extend to infinity. Numerical solutions are available to overcome these difficulties. These solutions can deal with localized defects, nonlinear materials, and other dynamics of the photonic crystal system [8,16,17]. Examples include the transfer matrix method and FDTD approaches. These methods often require large amounts of computational

power and time. It is increasingly possible to fabricate photonic crystals virtually instantaneously through laser induced photopolymerization, therefore it is desirable to develop another method for analyzing these structures, which can take into account various materials and show order of magnitude results in real time. To accomplish this a Split-Step Beam Propagation Method (BPM) approach was designed. A description of the eigenvalue solution and a BPM approach follows, along with a comparison of their respective results.

1.1 Band Structure Calculations the Generalized Eigenvalue Approach

Due to the periodicity of these materials the Bloch wave analysis is used to solve the wave equations. Solutions to the wave equations are the Bloch wave functions, which, according to the Bloch theorem, are periodic with the same periodicity as the medium in question [18]. Scalar or vector analysis can be used to calculate the band structure for a photonic crystal and both methods provide results consistent with experiment [1,4-15]. Due to its simplicity the scalar approach is utilized here. Scalar Maxwell's equations are satisfied when the incident field polarization is parallel to the features of a two-dimensional periodic structure and are used to derive the wave equations for the cases of an incident transverse electric (TE) or transverse magnetic (TM) wave [8]. In the case of a TM wave the electric field is oriented parallel to the symmetry axis while the inverse is true for the case of the TE wave. Wave equations for both cases are as follows:

$$\nabla^2 E - \frac{1}{c^2}\varepsilon(x)\frac{\partial^2 E}{\partial t^2} = 0 \qquad (1.1.1)$$

$$\nabla \cdot \frac{1}{\varepsilon(x)}\nabla H - \frac{1}{c^2}\frac{\partial^2 H}{\partial t^2} = 0 \qquad (1.1.2)$$

Equation 1.1.1 describes the case of the electric field polarized along the symmetry axis, TM, and forms a generalized eigenvalue problem, $Ax=\lambda Bx$, because the frequency eigenvalues are multiplied by the periodic dielectric function [8]. Equation 1.1.2 describes the case for the magnetic field polarized along the symmetry axis, TE, forming an ordinary eigenvalue problem [8].

Photonic crystals are in fact macroscopic crystals and their periodicity lends them to Fourier analysis. Wavevectors are always drawn in Fourier space, so that every position in Fourier space may have a meaning as a description of a wave [16]. In this case the dielectric function is periodic in r and has the following property:

$$\varepsilon(r+T)=\varepsilon(r). \qquad (1.1.3)$$

T is equal to one period of the dielectric function. In Cartesian coordinates, for the case of a two-dimensional crystal, ε(r) is periodic only in the x and y directions.

A simple case to begin with is a structure which is periodic in one dimension, with a lattice constant, a, in the x direction. Fourier expansion of the dielectric function, which is essentially a square wave, is as follows [18]:

$$\varepsilon(x) = \varepsilon_0 + \sum_{p>0}\left[C1_p \cos(2\pi Lx/a) + C2_p \sin(2\pi Lx/a)\right]. \qquad (1.1.4)$$

L is a positive integer and $C1_p$ and $C2_p$ are real Fourier coefficients and $2\pi/a$ gives the dielectric function, ε(x), a period of a [18]. The points $2\pi L/a$ are lattice vectors in reciprocal space, also known as Fourier space, of the crystal and describe the allowed terms in the Fourier series. Equation 1.1.4 can be written [18]:

$$\varepsilon(x) = \sum_l \varepsilon_l e^{i2\pi Lx/a} . \tag{1.1.5}$$

Multidimensional cases can easily be accommodated. A vector set G must be found such that

$$\varepsilon(r) = \sum_G \varepsilon_G e^{iG\cdot r} \tag{1.1.6}$$

is invariant under crystal translations T that leave the crystal invariant [16]. G is the reciprocal lattice vector.

Reciprocal lattice vectors can be constructed from the primitive vectors of the crystal lattice through the relationships in equation 1.1.7 [18].

$$G_1 = 2\pi \frac{b_2 \times b_3}{b_1 \cdot (b_2 \times b_3)} \qquad G_2 = 2\pi \frac{b_3 \times b_1}{b_1 \cdot (b_2 \times b_3)} \qquad G_3 = 2\pi \frac{b_1 \times b_2}{b_1 \cdot (b_2 \times b_3)} \tag{1.1.7}$$

Primitive vectors of the crystal are b_1, b_2, and b_3 and G_1, G_2, G_3, are the primitive vectors of the reciprocal lattice. G_1, G_2, and G_3 also have the following property.

$$G_i \cdot b_j = 2\pi\delta_{ij} \tag{1.1.8}$$

Only one reciprocal lattice vector exists for the one-dimensional case and it has the value:

$$G_1 = \frac{2\pi}{a} . \tag{1.1.9}$$

The variable, a, is the period of the one-dimensional photonic crystal.

Plotting the band structures using the above approach can become very time consuming. To avoid this, for the one-dimensional case, a simple but accurate solution to calculate the allowed frequencies can be derived from the Kronig-Penny model. A detailed description is found in reference *8*. From this analysis the following dispersion equation is derived:

$$\cos ka = \frac{(Z_1+1)^2}{4Z_1}\cos(k_1d_1+k_2d_2) - \frac{(Z_1-1)^2}{4Z_1}\cos(k_1d_1-k_2d_2) \qquad (1.1.17)$$

$$Z_1 = \frac{\sqrt{\varepsilon_1\mu_1}}{\sqrt{\varepsilon_2\mu_2}} \qquad (1.1.18)$$

In each region the wave number is given by k_1 or k_2 and d_1 and d_2 give the length of each region. The period of the material is a and the wave vector is given by k. The dielectric permittivity in each medium is ε_1 and ε_2 and the magnetic permeability in each medium is μ_1 and μ_2, respectively. Results of this solution are consistent with those provided by the analytical approach presented above and the run time of the program is significantly less.

In the two-dimensional case the reciprocal lattice vectors, G_1 and G_2, are of interest. The reciprocal lattice is constructed by summing combinations of the two basis reciprocal lattice vectors and is illustrated in figure 1.1.1 along with the crystal lattice in real space, for the triangular matrix.

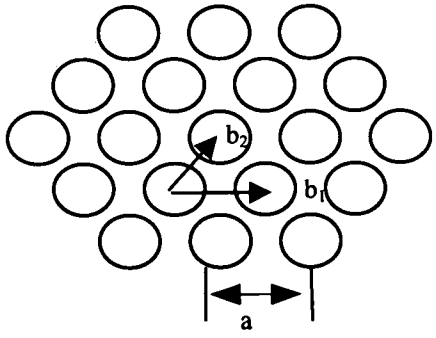

1.1.1a Triangular Lattice

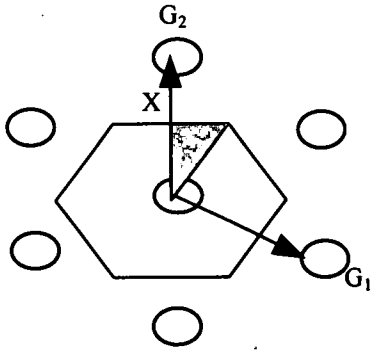

1.1.1b Reciprocal Lattice

Figure 1.1.1. Triangular lattice, 1.2.2a with period **a** and Reciprocal lattice 1.1.1b with primitive vectors. The boundary of the first Brillouin zone is shown in figure 1.1.1b.

Lattice vectors for the triangular lattice are as follows [8]:

$$b_1 = a\hat{e}_x \tag{1.1.9}$$

$$b_2 = \frac{a}{2}\hat{e}_x + \frac{\sqrt{3}a}{2}\hat{e}_y . \tag{1.1.10}$$

Lattice vectors for the reciprocal lattice are as follows [8]:

$$G_1 = \frac{2\pi}{a}\left(\hat{e}_x - \frac{1}{\sqrt{3}}\hat{e}_y\right) \tag{1.1.11}$$

$$G_2 = \frac{4\pi}{\sqrt{3}a}\hat{e}_y . \tag{1.1.12}$$

The first Brillouin zone is constructed in the reciprocal lattice and is shown as an outlined hexagon. The boundary is assembled by selecting a vector, G, from the origin to a reciprocal lattice point. A line is drawn normal to G and bisecting G, forming a boundary of the zone. This is repeated until a closed zone is constructed. Three symmetry points on the boundary exist and are labeled J, X,

and Γ, which describe the irreducible Brillouin zone. The entire Fourier space of the crystal can be constructed of the irreducible Brillouin zones.

Analysis in Fourier space requires the Fourier transformation of equations 1.1.1 and 1.1.2 and the insertion of the transform of the dielectric function. From the Fourier expansion of equation 1.1.5 the transform of the dielectric function is [16]:

$$\varepsilon(r) = \sum_{G} \varepsilon(G) e^{iG \cdot r}. \tag{1.1.13}$$

G is a vector in reciprocal space, which is constructed from the basis vector, G_1 and G_2, of the reciprocal lattice. Insertion of equation 1.1.13 into the Fourier transform of equations 1.1.1 and1.1.2 produces the following eigenvalue problems [8].

$$-|k+G|^2 E_G + \left(\frac{\omega}{c}\right)^2 \sum_{G} \varepsilon(G-G') E_{G'} = 0 \tag{1.1.14}$$

$$-(k+G) \cdot \sum_{G'} (k+G') \varepsilon^{-1}(G-G') H_{G'} + \left(\frac{\omega}{c}\right)^2 H_G = 0. \tag{1.1.15}$$

Eigenvalue problems such as these are best solved with a computer where large matrices are easily dealt with. Due to the scalar nature of the problem the eigenvectors are initially ignored, simplifying the process. Calculations are only carried out inside the first Brillouin zone as a result of the symmetry of the crystal. All of the wave vectors inside this space are of interest and each wavevector is constructed from the reciprocal lattice vectors. A matrix describing

the dielectric geometry in Fourier space is constructed using the wave vectors and the following equation, which is the Fourier transform of the dielectric function [8].

$$\varepsilon(G) = \varepsilon_b \delta_{G,0} + 2\beta(\varepsilon_a - \varepsilon_b)\frac{J_1(Gr)}{Gr} \tag{1.1.16}$$

$J_1(Gr)$ is the first order Bessel function and β is the fill ratio of the channels to the unit cell, in real space. The dielectric constants of the channel and substrate material are ε_a and ε_b. In the TM case this matrix serves as B in the eigenvalue equation while the diagonalized matrix $|k+G|^2$ serves as A. The returned eigenvalues, λ, for each wavevector, correspond to $(\omega/c)^2$. All propagation directions in the crystal can be accounted for by propagating along the vectors describing the boundaries of the irreducible Brillouin zone. Eigenvalues are calculated for k vectors lying on these vectors. Plotting the returned eigenvalues with respect to the k vectors produces the band structures.

1.2 Beam Propagation Method for Photonic Crystal Structures

Some limitations exist for the eigenvalue problem described above. As mentioned before a major limiting factor is the premise that the stuctures in question extends to infinity. This is therefore not neccesarily a solution for real world problems. Incorporation of defects and optically active materials in the structures is also prohibitive with this approach. Modeling of these structures with the inclusion of linear and nonliner materials is of interest, requiring another solution for the propagation of electro-magnetic waves through photonic crystals. Although several methods exist to numerically model these structures, it is my intention to develop a numerical solution that will provide addiquite results in as

little time as possible and take into account nonlinearities, materials with gain, defects, and other aspects of photonic crystal structures [8,16,17].

The split step BPM is a numerical simulation of an electromagnetic field as it propagates through a given medium and has been used extensively for the examination of materials presenting difficulties for analytical modeling [19-23]. BPM is commonly used for analyzing optical fibers and grating structures, in addition to nonlinear materials [22-28]. In the split-step BPM the medium is sliced into many thin elements so propagation and any modulation effects can be taken into account separately. Maxwell's wave equations are solved discretely to extract the equations for the propagation. From Maxwell's equations the Helmholtz equation, without any source terms, is as follows [19]:

$$\nabla E(x,z) + k^2 E(x,z) = 0 \tag{1.2.1}$$

Variable z is the propagation direction and x is transverse to this. The equation is Fourier transformed to solve for the angular spectrum [19].

$$\frac{\partial_z \xi}{\partial z^2} + \left(\frac{2\pi n}{\lambda}\right)^2 \left[1 - \alpha^2\right] \xi = 0 \tag{1.2.2}$$

$$\alpha \approx \frac{\lambda f_x}{n} \tag{1.2.3}$$

The refractive index of the material is given by n, the wavelength of the propagating field is λ, and f_x is a component of the angular spectrum of the field. The solution to equation 1.2.2 is given by [19]:

$$\xi(f_x, z) = \xi(f_x, 0) e^{i\frac{2\pi n}{\lambda}\sqrt{1-\alpha^2}z} \tag{1.2.4}$$

At each step the field is Fourier transformed and multiplied by the quadratic phase-factor, due to diffraction, associated with propagating a distance dz [19].

$$\xi_{out}(f_x, z+dz) = \xi_{in}(f_x, z)e^{-i\frac{\pi\lambda}{n}f_x^2} \tag{1.2.5}$$

The field is then inverse Fourier transformed and any additional phase or amplitude modulation factors are applied to the field. This process is repeated until the field has been propagated through the entire distance of the medium in question. An illustration of the slicing of the medium is shown in figure 1.2.1. Reflections at index interfaces should be taken into account to more exactly model the propagating field. This is fairly simple in the one-dimensional case where the medium consists of planes of alternating dielectric constants. In the two dimensional case this is some-what more difficult due to the cylindrical shape of the channels which will scatter light in a 180° arc. For this reason two slightly different approaches to the beam propagation method were used for the one-dimensional and two-dimensional cases. In addition, history is omitted due to the fact ultrashort pulse are being modeled. History is the result of the front end of a pulse causing the optical properties of the material to change. The back end of the pulse will then experience these changes as the pulse propagates. When dealing with ultrashort pulses, it is necessary to slice the medium into ultra-thin elements in order to take

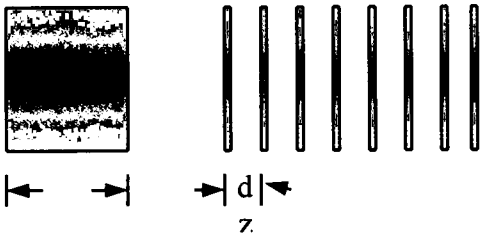

Figure 1.2.1 Slicing of the medium

into account the changes in material properties within the spatial pulse length, therefore these effects will initially be ignored.

1.3 BPM for One Dimensional Photonic Crystals

In a one-dimensional photonic crystal any light normally incident on the material either propagates through the material or is reflected, assuming it is a loss-less material and there is no scattering. This ideal case is modeled with a BPM code by propagating a beam through the material while taking into account the portion of the field that is back reflected to the input by Fresnel reflections at the index interfaces. Fresnel reflection coefficients and transmission coefficients are shown in equations 1.3.17a, 1.3.17b, 1.3.18a, and 1.3.18b [30]. Phase due to the reflections and any diffraction effects are taken into account in this method.

$$r_s = \frac{n_1 \cos(\theta_i) - n_2 \cos(\theta_t)}{n_2 \cos(\theta_t) - n_1 \cos(\theta_i)}, \qquad t_s = \frac{2n_1 \cos(\theta_i)}{n_2 \cos(\theta_t) + n_1 \cos(\theta_1)} \tag{1.3.17}$$

a b

$$r_p = \frac{n_2 \cos(\theta_i) - n_1 \cos(\theta_t)}{n_1 \cos(\theta_t) - n_2 \cos(\theta_i)}, \qquad t_p = \frac{2\frac{n_1}{n_2}}{1 + \frac{n_1 \cos(\theta_t)}{n_2 \cos(\theta_i)}} \tag{1.3.18}$$

a b

The angles θ_i and θ_t are the incident and refracted angles of the field, respectively. At each interface, between regions, a portion of the field, proportional to the reflection coefficient, is reflected. After reflection the fields are propagated back through the medium, accumulating the appropriate phase. A summation over all of the fields is performed to determine the constructive and destructive behavior

of the propagating waves and the magnitude is found to determine the reflected intensity. To determine the transmitted wavelengths the intensity of the reflected light is subtracted from the intensity of the input. This can be done as a result of conservation of energy. In a loss-less material, any wavelengths of light, which do not appear back at the input, must be transmitted through the material.

1.4 BPM for Two Dimensional Photonic Crystals

Modeling a two-dimensional photonic crystal offers some unique challenges in comparison with the one-dimensional case. Phase modulation and reflections will occur in two dimensions, making it difficult to account for all of these factors. In this model the preliminary steps have been taken to formulate a BPM simulation for two-dimensional photonic crystals. As a first approximation in the algorithm, reflections at the index interfaces are ignored and only the phase accumulation due to the index modulation is taken into account. In doing this only the diffractive and refractive properties of the material are examined.

To model the photonic crystal the medium is sliced in both of the inhomogenous dimensions to produce a rectangular matrix containing the appropriate values of the indices of refraction. The index of each array element is dictated by the location of the element relative to the channel radius. Matrix elements lying inside the channel are assigned the value of the index of the channel material and those elements outside of the channel are assigned the index value of the matrix material. Two cells are constructed containing the channels surrounded by a rectangle of dimensions equal to the channel spacing. In the

triangular lattice the channels are shifted by a/2 in every other row so two primary cells were constructed to compensate for this. The cells were rectangular with dimensions of a by $a\sqrt{3}/2$, where a is the spacing of the cylinders. One cell contains the channel at its center and the other cell has the channel positioned at its edges. These cells are illustrated in figure 1.4.1.

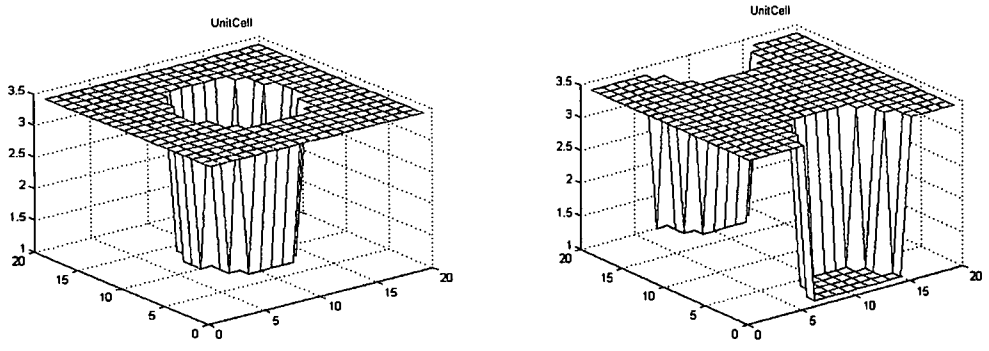

Figure 1.4.1. Unit cells for both cases. a) Cell for first row of channels. b) Cell for second row of cells

A one-dimensional unpolarized Gaussian beam was propagated through the material. In order to propagate a beam with a reasonable beam waist, propagation cells were constructed which consisted of an array of the above cells, for each row of channels. These were the main propagation cells and are illustrated in figure 1.4.2.

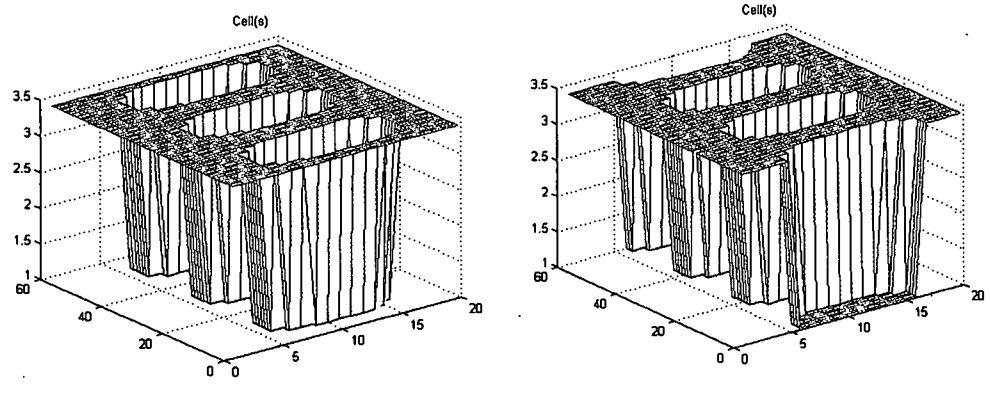

Figure 1.4.2. Propagation Cells for each row of channels

The main propagation cells were set up to have a width several times the size of the beam waist to reduce any diffraction effects of the finite aperture.

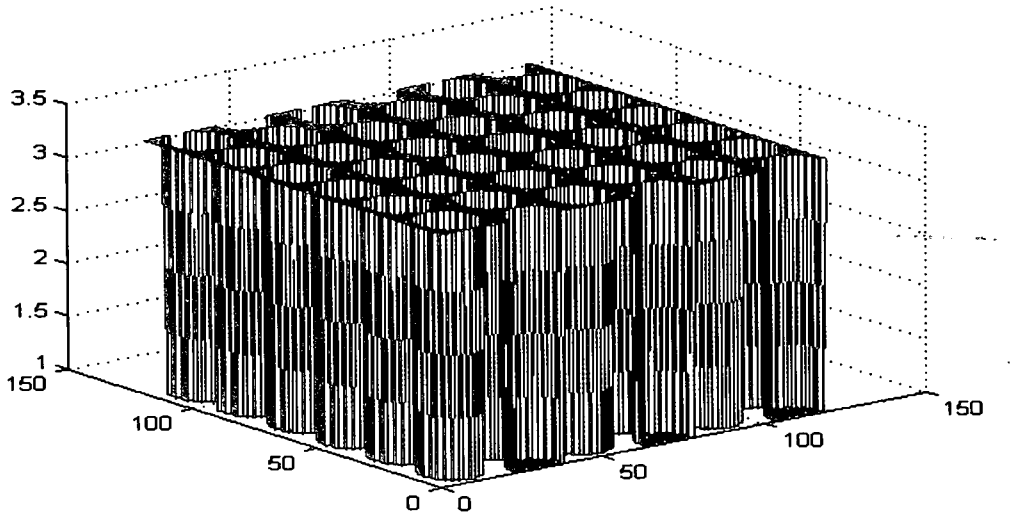

Figure 1.4.3. Representation of a portion of the photonic crystal index profile

Figure 1.4.3 shows the index profile for several cells and is representative of a portion of a photonic crystal.

Propagation through the main cell was performed in a direction perpendicular to the long axis of the main propagation cell array. The field was stepped through the cell one longitudinal array element at a time, accumulating the appropriate phase due to the index at each transverse array element. The quadratic modulation phase had the following form.

$$ModulationPhase = e^{-i*\frac{2\pi}{\lambda} Maincell_n(:,m)} \qquad (1.4.17)$$

Maincell(:,m), the propagation cell, contains all of the appropriate index information including any nonlinearities. The *m* represents the BPM loop index and steps the field through the cell. After propagating through one of the main cells the output of this field is used as the input for propagation through the next row of columns. The field was propagated through four to six rows of columns, corresponding to a distance of approximately 4.5-μm in this example. This distance was shown to be long enough to see effects of the periodic refractive index on the field. Transmission notches will increase in depth as the field is propagated farther into the material but using longer distances slows the program and introduces adverse diffraction effects due to the finite aperture.

A beam propagating through the length of a crystal will diffract even if the crystal index were homogenous. In order to distinguish the effects of the periodic index from the effects of normal diffraction a beam was propagated through a homogenous medium of length equal to that of the photonic crystal with a refractive index equal to the matrix material. A range of fields, with varying wavelengths, was propagated through the crystal to establish the wavelength dependence of the transmission. At the output of the crystal the magnitude of the field was found and an integration was performed over the beam to get a value proportional to the transmitted power. The power of the field exiting the periodic crystal was then normalized to the power of the field transmitted through the homogenous medium.

1.5 One Dimensional Lattice: Eigenvalue Solution and BPM Results

Calculations were performed for a one-dimensional photonic crystal with index contrasts of 1:1.2 and 1:3.605. Figures 1.5.1 and 1.5.2 illustrate the band structure for a 1D crystal with dielectric layers of equal thickness for index contrasts of 1:1.2 and 1:3.605 respectively. These dimensions and indices were chosen for comparison with published results [1,8]. The following plots, for the one-dimensional case, were produced with a solution based on the Kronig-Penny model discussed in section 1.1. These results are consistent with the results produced by solutions based on the variational theorem and the eigenvalue approach.

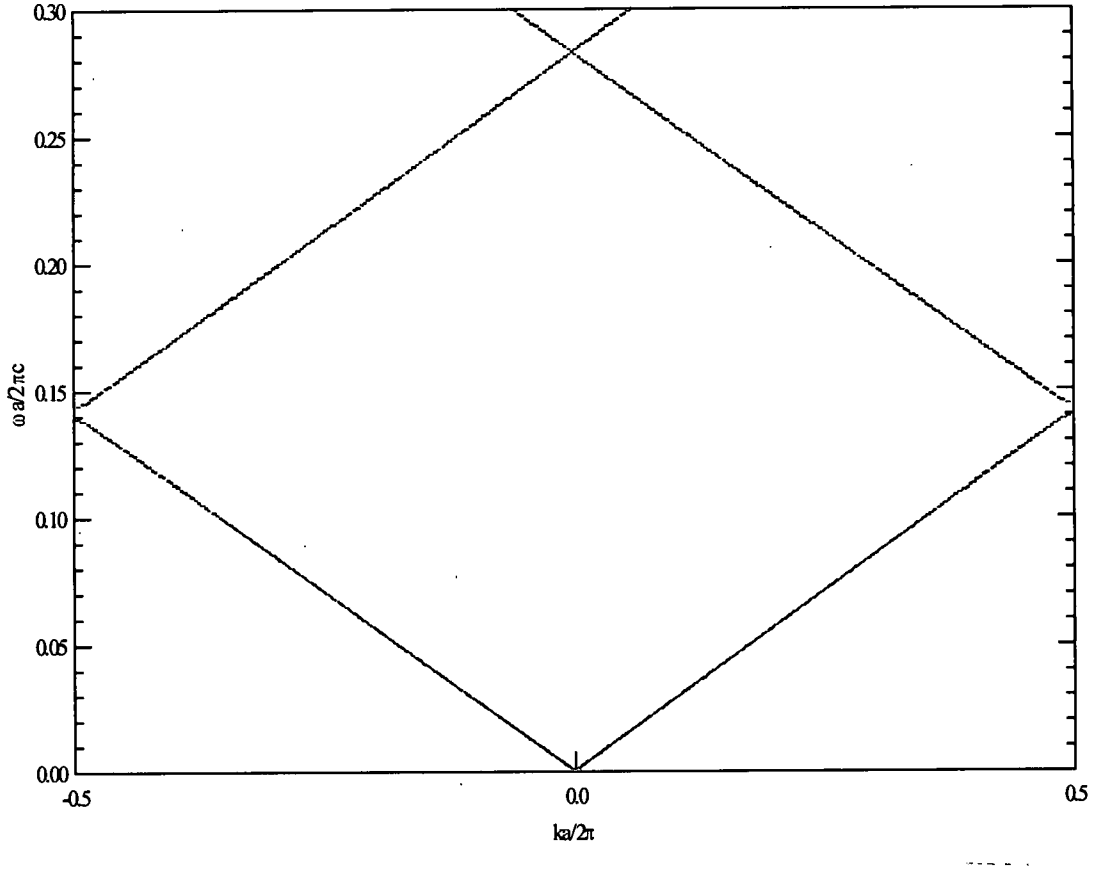

Figure 1.5.1. Eigenvalue band structure for a 1D crystal with equal distance regions and an index contrast of 1.0:1.2.

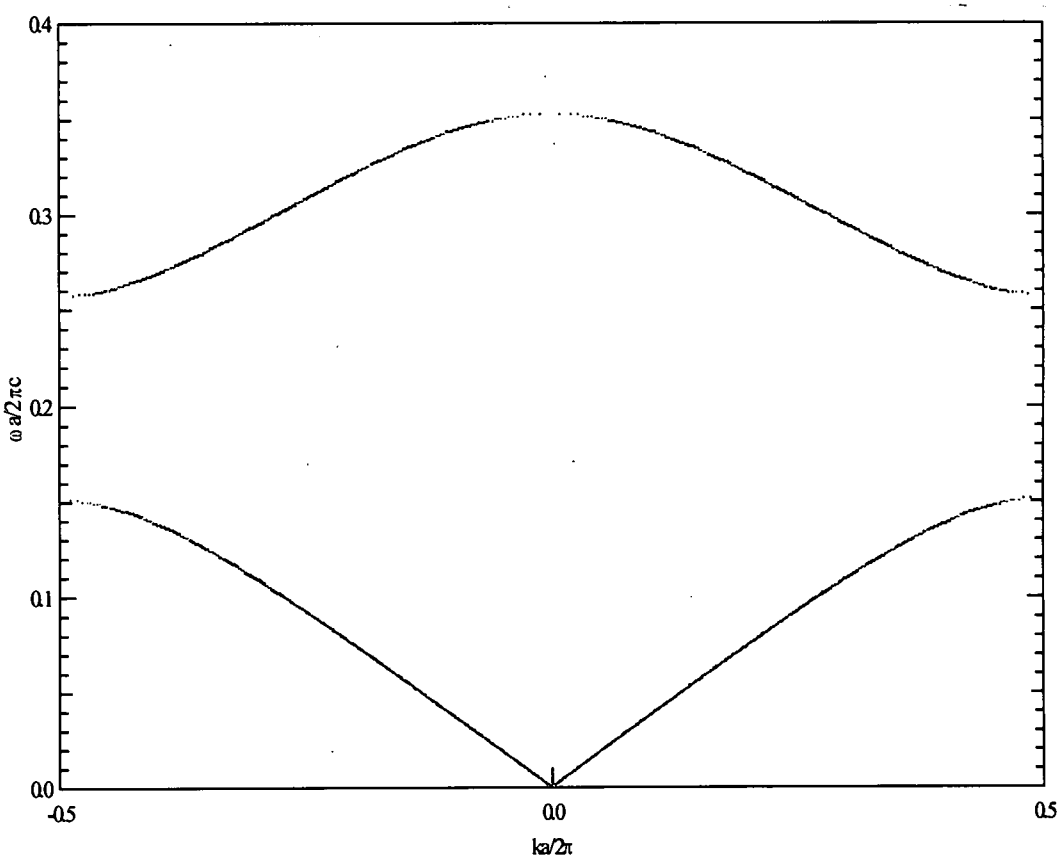

Figure 1.5.2. Eigenvalue band structure for a 1D crystal with equal distance regions and an index contrast of 1.0:3.605

Due to the scalable nature of the photonic crystals these band structures are relevant for any one-dimensional photonic crystal with equal distant regions and index contrasts of 1.0:1.2 and 1.0:3.605. Wavelengths falling in the gap can be calculated by dividing the periodicity, a, by the appropriate y coordinate. A band gap will always appear for a one-dimensional crystal when the ratio of the dielectric constants is not equal to 1. It is apparent from these band structures that the gap width increases with an increase in the dielectric contrast. In figure 1.5.1 the first bandgap is very small and is centered at a wavelength of $a/0.14$. In figure 1.5.2 the first bandgap is centered at a wavelength of $a/0.205$ and has a width of

approximately a/0.26 to a/0.15. These results are consistent with the results reported in literature [1,8]. It is apparent from the plots that the gaps occur at the edge or at the center of the Brillouin zone. At the edge of the Brillouin zone $k = \pi/a$, which corresponds to a wavelength twice the lattice constant, $2a$. Bandgaps are a result of this phenomenon and this concept will be discussed in section 1.6.

For comparison with the BPM results the eigenvalue band structure was extended over a wide range of wavelengths. Figure 1.5.3 illustrates the band structure for a material with a refractive index of 1.0 in the first region and 3.605 in the second region. A period of 600 nm with equal distant regions was arbitrarily chosen and the results are plotted over a wavelength range from 500 nm to 4 μm. The field was propagated through 25 layers of the medium, which corresponds to approximately 7.5 μm. To give a better understanding of how the gaps from the eigenvalue solution align with the transmission valleys of the BPM results both are plotted on the same graph.

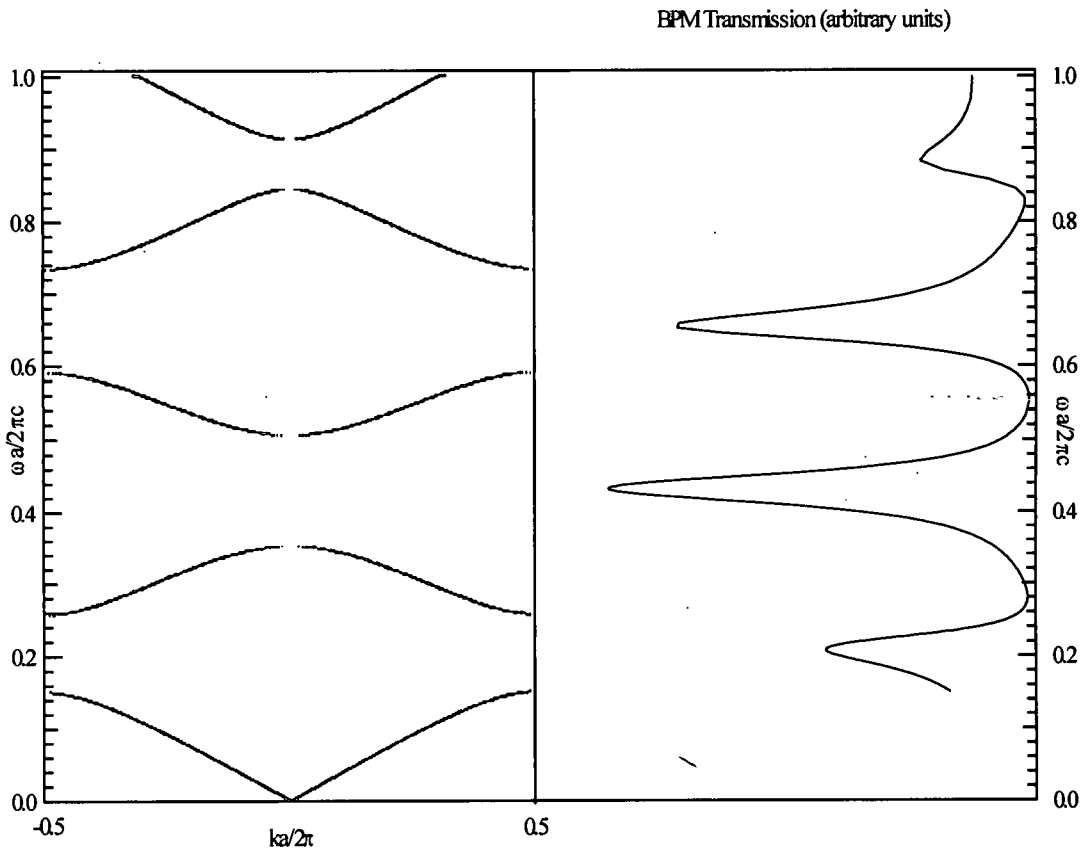

Figure 1.5.3. Eigenvalue solution and BPM results for a 1D photonic crystal with equal distant regions and indices of 1.0 and 3.605. BPM is on the right had side of the plot.

At the band gap wavelengths the transmission from the BPM is reduced by a considerable percentage. Results from the BPM are consistent with those from the eigenvalue solution with gaps for both solutions appearing at approximately 681 nm, 909 nm, 1.36 μm, and 3.0 μm.

1.6 The Photonic Band Gap

Band gaps occur at the center or at the edge of the Brillouin zone as illustrated in figure 1.5.2. At the edge of the Brillouin zone the wavelength corresponds to $2a$, twice the lattice constant of the photonic crystal. In essence the wave is standing with its nodes in either the high dielectric or low dielectric material [1]. The focus of the explanation is on the first two bands of the band structure presented in figure 1.5.2. A one-dimensional photonic crystal with a standing wave in the material is illustrated in figure 1.6.1. Shaded areas represent the larger refractive index. From the electro-magnetic variational theorem it is known that low-frequency modes concentrate their energy in high dielectric regions while the inverse is true for high frequency modes[1]. It is also known that as a wave propagates through a material the frequency does not change but the wavelength changes according to the index of refraction. This also means that two waves of the same wavelength, each propagating through a different refractive index, must each have a different frequency. If a wave is positioned so its nodes are in the high dielectric region then most of its energy will be concentrated in this region. The index of refraction encountered by the wave will be that of the material in which its energy is concentrated. At the edge of the Brillouin zone the two modes have the same wavelength but due to the regions in which their energy is concentrated the two waves will have differing

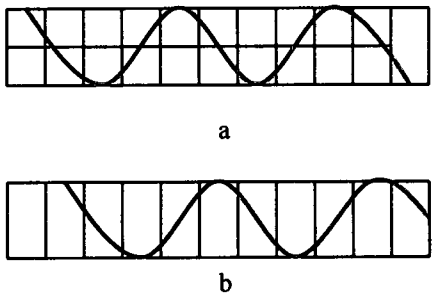

Figure 1.6.1. Modes for the firs two bands of a one-dimensiona photonic crystal. Figure 12a i the first band while figure 12b i the second band

frequency. Due to the higher index seen by the mode of figure 1.6.1a, the frequency is lowered somewhat from the frequency of the wave that has its energy concentrated in the lower dielectric regions, thus a gap forms. As the dielectric contrast is increased the frequency difference will increase as well, therefore larger bandgaps occur for larger dielectric constants.

1.7 Two Dimensional Triangular Lattices: Eigenvalue and BPM Results

Band structure calculations were performed for a two-dimensional triangular lattice with 0.72 μm diameter channels of index 1.0, and a spacing of 0.75 μm with a matrix material index of 3.605. Again these values are chosen for comparison with published results [1,8]. The band structures for the TE and TM cases are shown in figures 1.7.1 and 1.7.2 respectively.

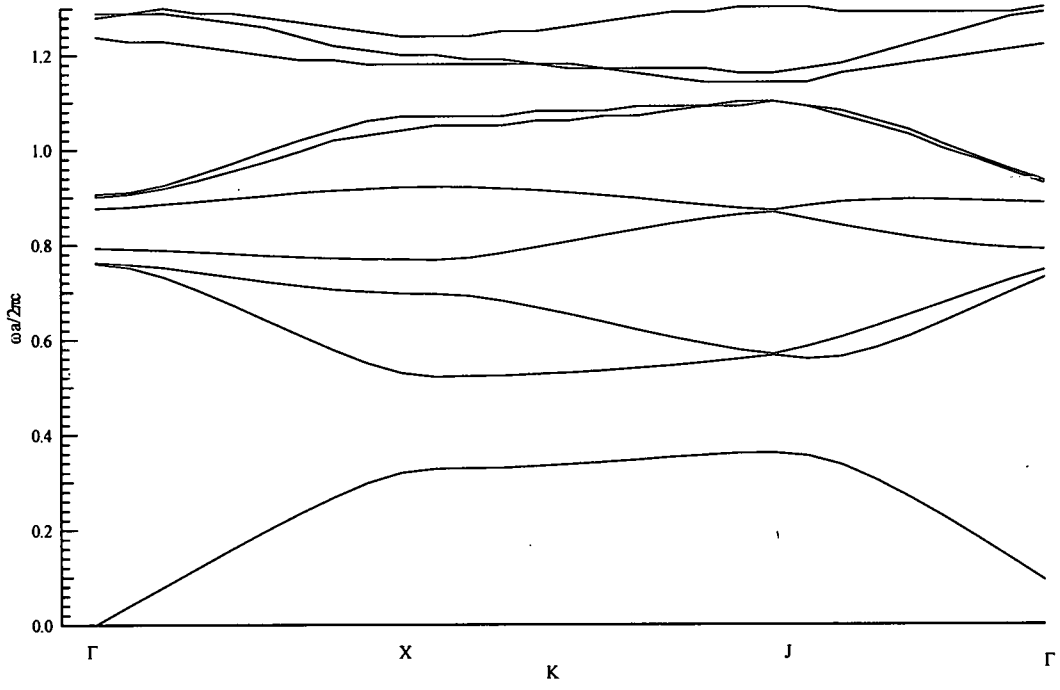

Figure 1.7.1. TE band structure for two-dimensional photonic crystal with r/a=0.48 and n1=1.0 and n2=3.605

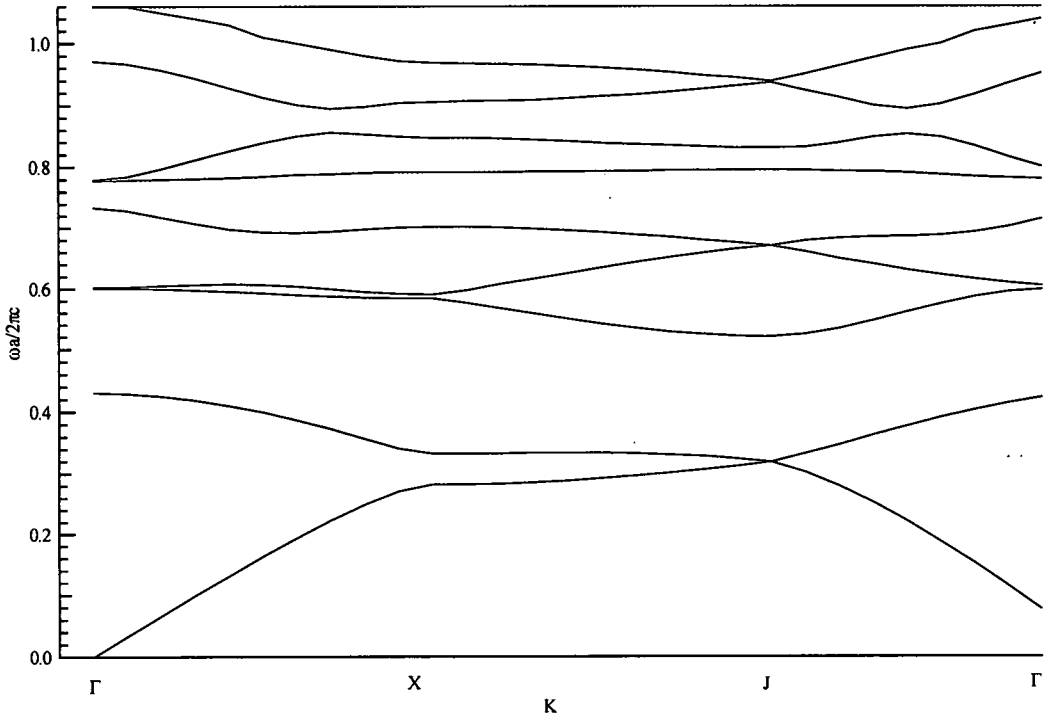

Figure 1.7.2. TM band structure for two-dimensional photonic crystal with r/a=0.48 and n1=1.0 and n2=3.605

Several gaps are present in the band structures. For the TE case a large gap exists between the first and second bands and another band gap is present between the seventh and eighth bands. A gap exists between the second and third bands and between the fifth and sixth bands for the TM case. The lowest bandgaps for both polarizations overlap indicating that no light, inside the gap, would propagate in the plane normal to the symmetry axis of the cylinders. The *y*-axis is $\omega a/2\pi c$ where a is the spacing of the cylinders. The *x*-axis is the propagation vector in reciprocal space with the symmetry points of the irreducible Brilouin zone labeled. Any structure with the ratio of the radius of the channels to the spacing, r/a, of 0.48 and an index contrast of 1.0:3.605 will show this band structure. Again this is due to the scalable nature of these structures. As this ratio

is decreased the width of the band gaps will decrease and eventually no gaps will exist. Gaps are also dependent upon the index contrast. The gap width will decrease with lower refractive index contrasts. Conversion to wavelength proceeds in the same fashion as with the one-dimensional case, divide the cylinder spacing, *a,* by the approriate *y* coordinate.

In this fist step of the BPM analysis a propagation direction is chosen which corresponds to the Γ-J direction in reciprocal space. As a result, in this model the band structure for all other propagation directions can be ignored. Calculated band structures for the TM and TE polarization when limited to the Γ-J direction are shown in figures 1.7.3 and 1.7.4. A photonic crystal structure with the same dimensions as those of the crystal modeled above was used for the BPM analysis. To better understand the behavior of the crystal a large number of bands were calculated and to illustrate the effects of the band gaps on the transmission, the BPM results and the analytical results are both shown on the figures. Due to the fact that the incident light is not polarized both band structures must be taken into account. The field was propagated through 10 rows of columns, which corresponds to approximately 7.5 μm.

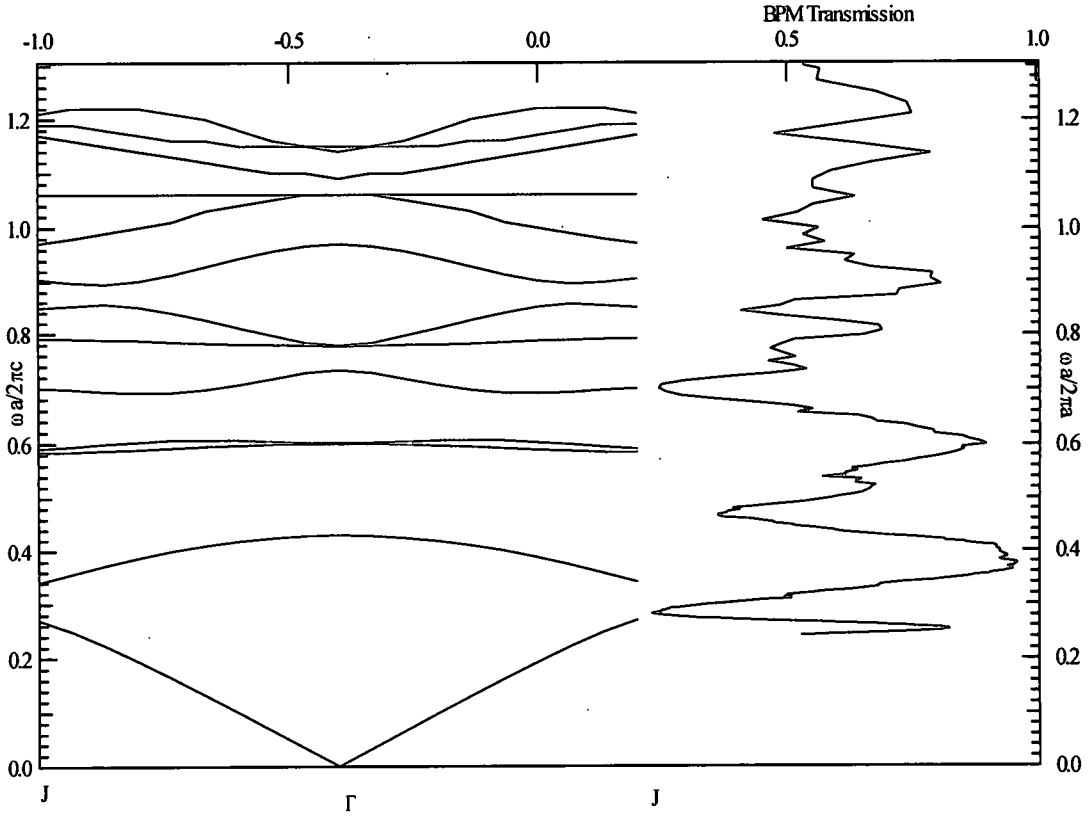

Figure 1.7.3. Eigenvalue and BPM for the TM case for a 2D photonic crystal with r/a=0.48a and nc=1.0 and nm=3.605

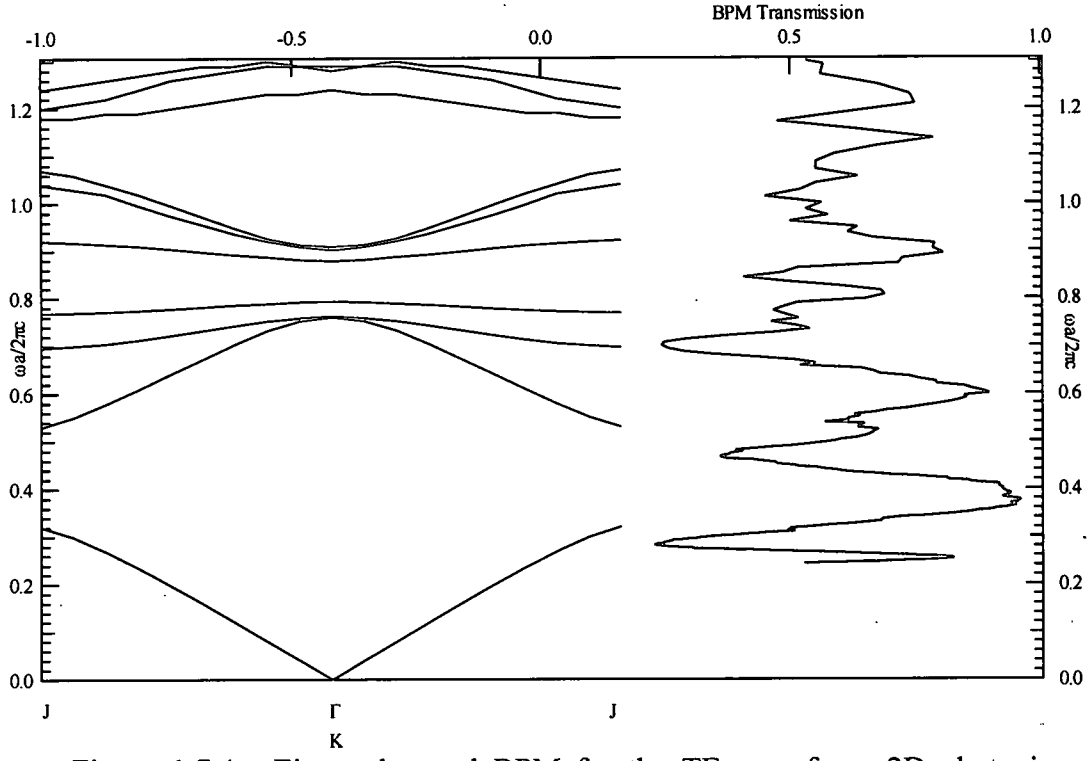

Figure 1.7.4. Eigenvalue and BPM for the TE case for a 2D photonic crystal with r/a=0.48 and nc=1.0 and nm=3.605

Several band gaps exist for this structure for the TE and TM cases. In the eigenvalue solution for the TM case three large gaps exist for wavelengths from 1.29 μm to 1.7 μm, 2.2 μm to 2.6 μm, and 1.08 μm to 1.21μm. Several other gaps are shown between 0.5 μm and 1.01 μm. The TE case shows gaps from 0.64 μm to 0.69μm, 0.86 μm to 0.69 μm, and 1.44 μm to 2.30 μm. Other small gaps exist for the TE polarization at 0.5 μm and 0.42 μm.

In the BPM analysis computational time limitations did not allow for a propagation window to compensate for beam waists much larger than 10 μm. Also, adverse diffraction effects will become apparent if a larger beam waist and a smaller window are employed for the propagation. The wavelength dependence of the transmission is illustrated in figure 1.7.3 and 1.7.4 on the right hand side of the plots. Three well-defined notches in the transmission exist corresponding to the large band gaps present on figures 1.7.3 and 1.7.4. It is apparent that the transmission is affected by the band gaps and the large notches in the transmission appear at approximately the same locations as the bandgaps of the analytical solution for the TM case. The noisy portion of the transmission plot is a result of the small, closely packed, band gaps at the shorter wavelengths. Inaccuracy and poor resolution due to computational limitations in modeling the photonic crystal resulted in the limited consistency between the eigenvalue solution and the beam propagation method. Figure 1.7.5 is a plot of the BPM output as a function of wavelength. An interesting feature of this figure is the structure on the right hand side. Further examination of this wavelength region divulged another notch in the transmission and is illustrated in figure 1.7.6.

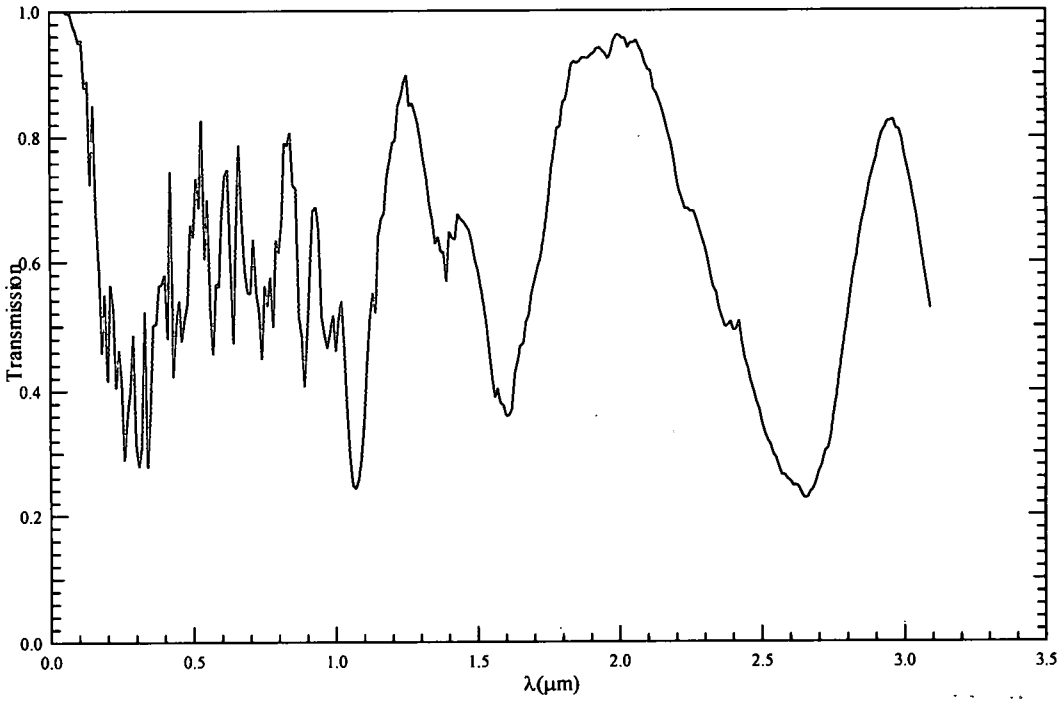

Figure 1.7.5. BPM results for a 2D photonic crystal with d=720nm and a=750nm and nc=1.0 and nm=3.605

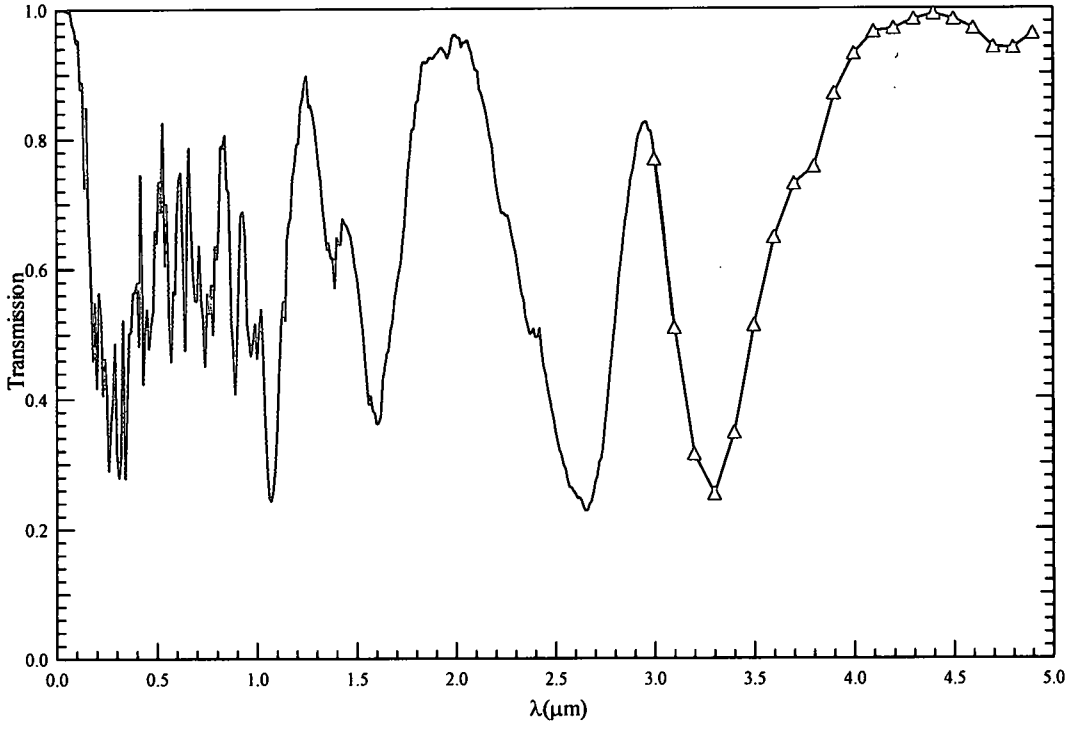

Figure 1.7.6. Extension of the BPM output to illustrate the second transmission notches at the longer wavelengths.

The line with markers represents the transmission of these additional wavelengths. According to the analytical solution these wavelengths propagate through the crystal uninhibited. A possible explanation for this occurrence is the fact that these features are harmonics of band gaps at shorter wavelengths. The large transmission notch at the right of the figure is centered at 3.3 μm. A harmonic of this is 1.65 μm and there is a large transmission valley present at this wavelength.

This BPM code is my first step toward numerically modeling these structures. To more accurately model a photonic crystal, reflections and scattering, among other factors, must be taken into account. A model such as this is desirable for the reason that it will be able to take into account the dynamics of a system that incorporates linear and nonlinear optically active materials The above results show progress towards accomplishing a reasonable model for these materials.

CHAPTER 2

Construction of Photonic Crystal Structures

Photonic crystals, which are functional in the range of optical radiation, must have features with dimensions on the order of the wavelength of light. Several techniques exist for the manufacture of these types of structures including; micro machining, holographic one-photon induced photopolymerization, holographic two-photon induced photopolymerization, and bias sputtering [31-36]. Holography is often associated with imaging but in the recent past this technique has been used for information storage as well as micro-scale and nano-scale fabrication [37]. Specifically, holographic two-photon induced photopolymerization (H-TPIP) has recently been examined as a viable technique for holographic recording and micro and nano-fabrication [29,30,32,33]. Holography utilizes the interference of coherent beams to store information inside a photographic material. In this method the interference of ultrafast coherent beams causes high intensity regions to exist at the recording medium in the form sinusoidal patterns, planes, columns, or isolated regions in a three-dimensional matrix. Fabrication of photonic crystals can be accomplished using this process with the periodicity in one, two, and three dimensions. In addition to these

methods, a technique has been devised at the Naval Research Laboratories (NRL) in Washington D.C. which produces two dimensional photonic crystals with air channels in a glass substrate. This method uses and iterative glass-drawing process to produce these structures. Construction of one-dimensional and two-dimensional photonic crystals is examined in the following.

2.1 Holographic Technique using Two Photon Induced Photopolymerization

In this holographic technique the number of beams required to produce a polymerized photonic crystal is the number of desired crystal dimensions plus 1. It is possible to cause photopolymerization in a one-photon [35,37] or two-photon process [31,32]. In the two-photon process the rate of polymerization has a quadratic intensity dependents as opposed to the one-photon case which is fluence dependent and is linear with respect to the intensity. Compared to the one-photon case, in the two-photon case the rate of polymerization at the high intensity regions is increased while the rate of polymerization is reduced at the low intensity regions. As a result of this, H-TPIP improves on single photon polymerization and other lithographic approaches by reducing the scale of the features, down to 1μm, and increasing the aspect ratio to greater than 50 [31]. In this experiment, NOA 72™ a photopolymerizable thiolene optical adhesive produced by the Norland Chemical Company, in combination with AF380 provided the recording medium. NOA 72 is cured with light ranging from 315 to 450 nm [31,38]. AF380, an Air Force material, has a strong up-converted luminescence centered at 500 nm [31]. A Ti:Sapphire femtosecond laser system was used to generate 90-fs,

950-μJ pulses centered at 790-nm with a repetition rate of 500 Hz. A thin lens in combination with one or two beam splitters, depending on the desired photonic crystal dimensions, were used to produce multiple beams with spot sizes of, 4 mm^2 to 10 mm^2, at the recording medium.

Very short pulses are broadband making it necessary to account for the interference of all of the frequencies contained in the beam. The pulses can be approximated as Gaussian and Fourier series decomposition is used to extract the frequency components and their amplitudes. The field at the image plane is the sum of all of the fields resulting from the different frequencies.

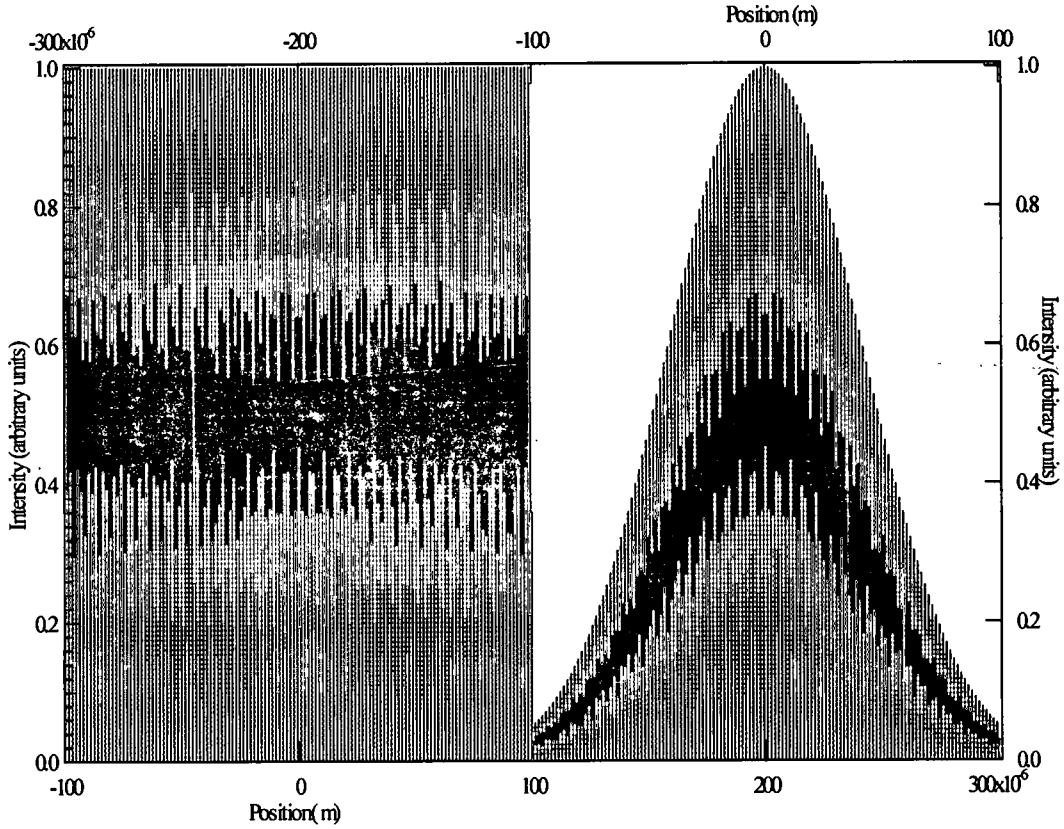

Figure 2.1.1 Intensity profile of the interference of two beams, left is a single wavelength, right is multiple wavelengths.

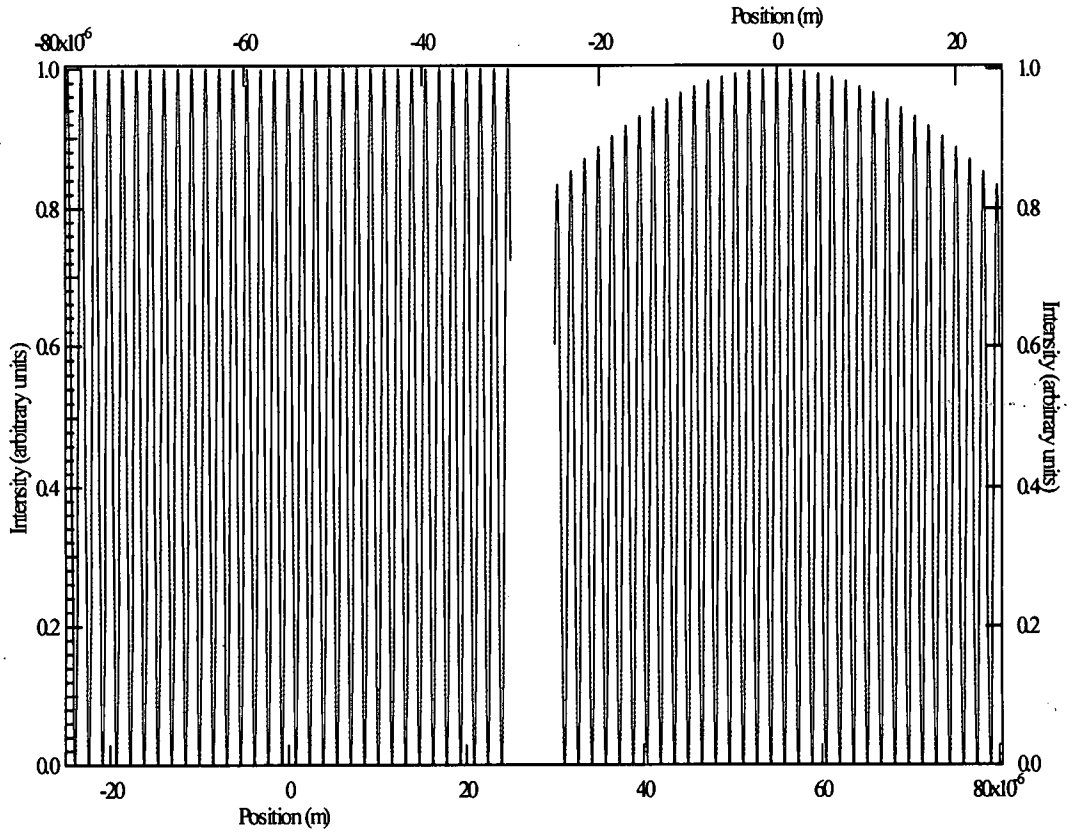

Figure 2.1.2 Intensity profile of the interference of two beams, left is a single wavelength, right is multiple wavelengths.

In figures 2.1.1 and 2.1.2 the intensity profile is shown for the center wavelength of the pulse and for the summation of several hundred frequencies. The angle subtended by the two beams is 30° with an arbitrary input intensity. Its is apparent that the profile has changed while the period has remained essentially the same. For clarity, only a section of the intensity pattern is shown, in actuality the spot extends over several hundred microns. The frequencies sum to produce a Gaussian profile due to the fact that the temporal and spatial profile of the pulse is approximately Gaussian. Figure 2.1.2 is a magnification of figure 2.1.1 to show the periodicity more clearly.

In addition, due to the coherence length and the angle of incidence of the beams, an area of maximum temporal overlap is observed at the center of the spot. In this area the sharpest gratings are present with the grating structure decreasing in definition with an increase in radius from the center. This area of peak intensity gives the spot a cats eye appearance. Plots of the intensity pattern, without the inclusion of interference patterns, are shown in figure 2.1.3. Figure 2.1.3a illustrates the Gaussian intensity profile for what is essentially a CW beam. Figure 2.1.3b on the other hand shows the cats-eye intensity pattern resulting from the temporal overlap of the two beams. Interference patterns are not shown on these figures for the sake of clarity.

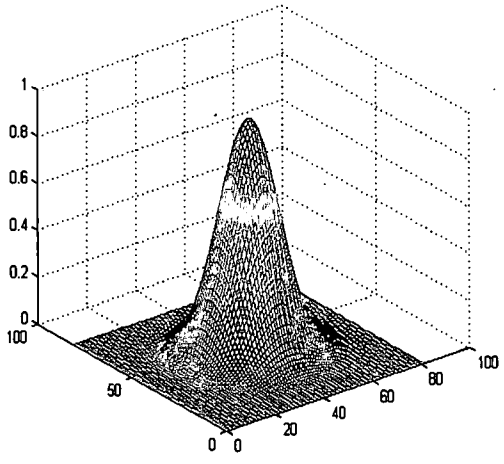

Figure 2.1.3a. Gaussian profile at the sample. Temporal effects of the beam are not accounted for.

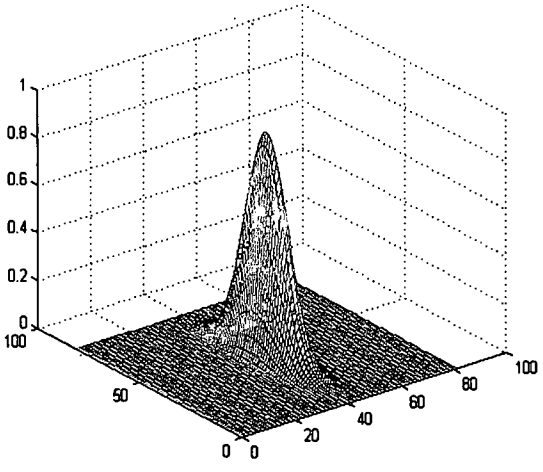

Figure 2.1.3b. Cats eye intensity profile resulting from the temporal effects of the pulse

In this setup, each beam propagates along a delay line, one with a translation stage to ensure proper temporal overlap of the beam. A 100 fs pulse

has a coherence length of approximately 30 μm in free space; therefore it is critical that temporal and spatial overlap be maintained. To ensure temporal overlap a KDP crystal was placed at the sample plane and the second harmonic was observed. By translating the delay stage the output of the second harmonic could be maximized, therefore maximizing the temporal overlap.

2.2 One Dimensional Photonic Crystal and a Thin Film Grating

Recording of grating structures utilized a variation of the Michelson interferometric setup illustrated in figure 2.2.1 [39,40]. The two fields at the recording media will have the following form [39].

$$E_1 = \frac{E_0}{\sqrt{2}} \exp\left[-jk\left(z\cos\left(\frac{\theta}{2}\right) + x\sin\left(\frac{\theta}{2}\right)\right)\right] e^{-jkL_1} e^{-j\Delta\phi} \tag{2.2.1}$$

$$E_2 = \frac{E_0}{\sqrt{2}} \exp\left[-jk\left(z\cos\left(\frac{\theta}{2}\right) - x\sin\left(\frac{\theta}{2}\right)\right)\right] e^{-jkL_2} \tag{2.2.2}$$

The recording medium is in the *x-y* plane. The angle θ is the angle subtended by the two beams and k is the wave number. E_0 is the field magnitude and j is imaginary. Phase differences between the beams is given by $\Delta\phi$ and, in this case, is assumed to be zero. The field component z is normal to the recording film and x is parallel to the recording medium. The path length of the two beams is L_1 and L_2. For a fixed z, the intensity at the recording medium will have the following form [39].

$$I = 2\left(\frac{E_0^2}{2}\right)\cos^2\left[kx\sin\left(\frac{\theta}{2}\right) + k(L_2 - L_1) + \frac{\Delta\phi}{2}\right] \tag{2.2.3}$$

The intensity will vary with a sinusoidal period of:

$$d = \frac{\lambda}{2\pi \sin\left(\theta/2\right)}. \tag{2.2.4}$$

The wavelength of the incident light is given by λ.

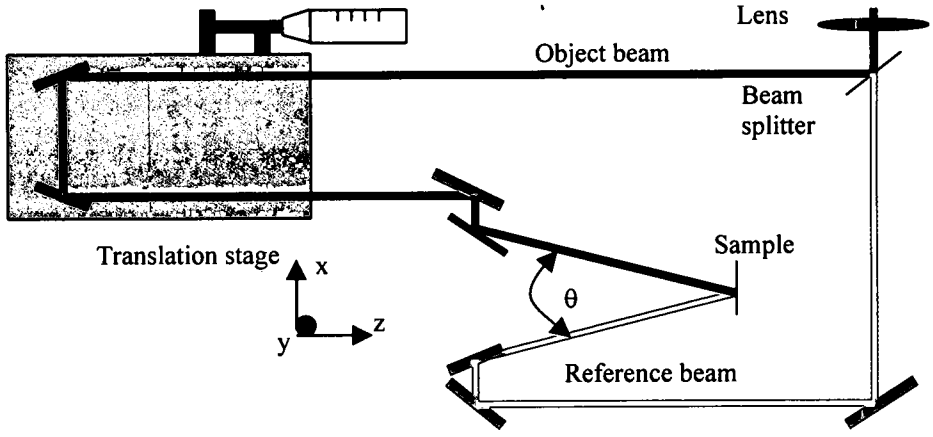

Figure 2.2.1 B. Holographic setup for a grating structure

To produce an intensity pattern with planes of constructive interference the optical set up of figure 2.2.1 was arranged to facilitate counter propagating beams and is shown in figure 2.2.2. This is the basis for constructing a one-dimensional photonic crystal. The fields at the recording medium are as follows.

$$E_1 = \frac{E_0}{\sqrt{2}} \exp\left[-jk\left(z\cos(\theta_1) + x\sin(\theta_1)\right)\right] e^{-jkL_1} e^{-j\Delta\phi} \tag{2.2.5}$$

$$E_2 = \frac{E_0}{\sqrt{2}} \exp\left[-jk\left(z\cos(\theta_2) + x\sin(\theta_2)\right)\right] e^{-jkL_2} \tag{2.2.6}$$

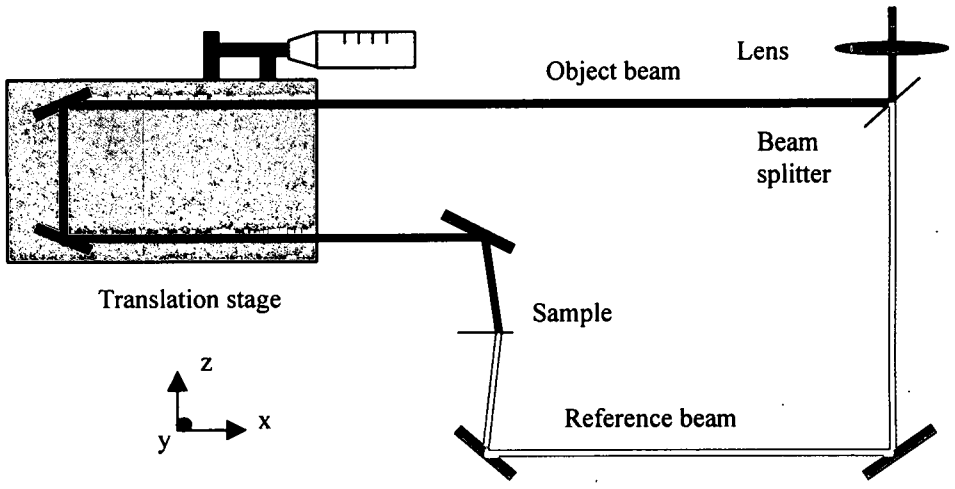

Figure 2.2.2. Holographic set up for a 1D photonic crystal

In this case the angles θ_1 and θ_2 are the angles measured off of the positive z-axis. Again the magnitude of the sum of the two fields is used to find the intensity at the recording medium. The intensity will vary periodically in the z and x directions and will have the following form.

$$I = 2\left(\frac{E_0^2}{2}\right)\cos\left\{k\left(z\left[\cos(\theta_1)+\cos(\theta_2)\right]+x\left[\sin(\theta_1)+\sin(\theta_2)\right]\right)\right\} \qquad (2.2.7)$$

Figure 2.2.3 illustrates the intensity pattern for two beams which propagate collinear along the z-axis.

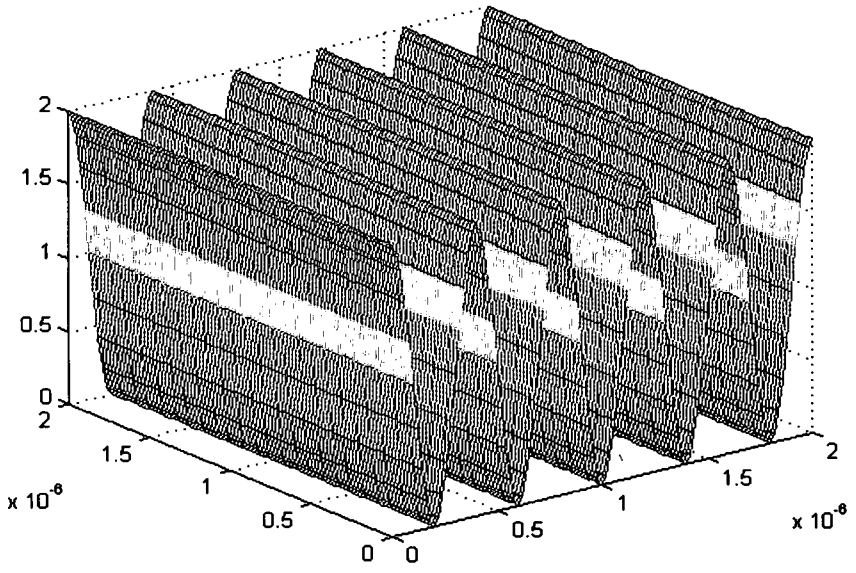

Figure 2.2.3. Illustration of the intensity pattern for the interference of two counter propagating beams. Units are μm on the x and z and arbitrary intensity units on the y.

This intensity pattern will produce planes of high intensity with a period of:

$$d = \frac{\lambda}{2\pi} \tag{2.2.8}$$

in the z direction. Adding any angle to the propagation direction of the beams will introduce a periodicity in both the z and x directions.

2.3 Construction of Two Dimensional Photonic Crystal using H-TPIP

Interference of three beams can produce a hexagonal two-dimensional intensity pattern. The periodicity and the shape of the intensity profile are dictated by the angle at which the three beams interfere and by the wavelength of

light. An intensity profile for the interference of three beams with two beams counter propagating collinear and the third beam normal to these is shown in figure 2.3.1. In this case the three beams have no y components.

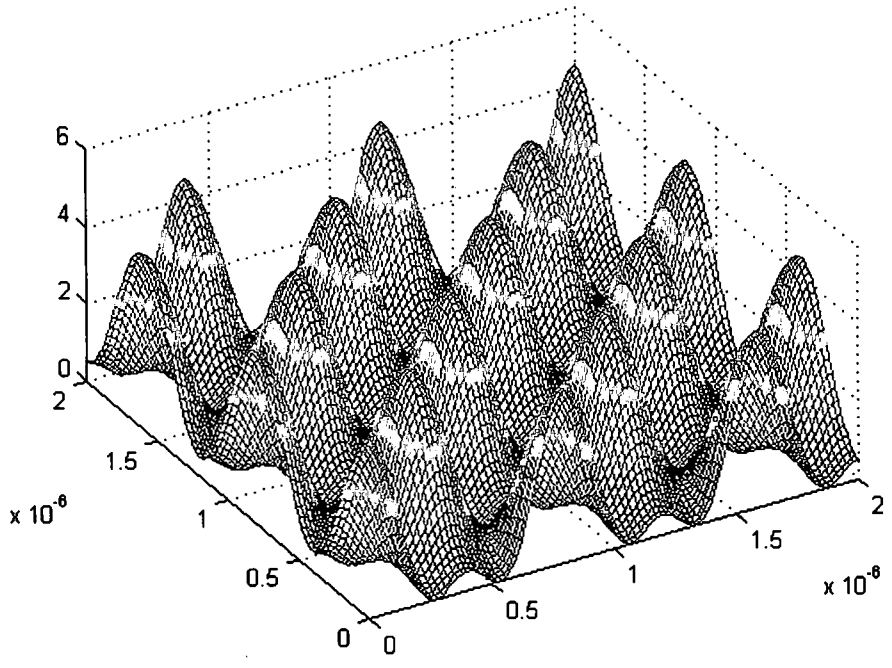

Figure 2.3.1. Intensity profile for the interference of three beams. Hexagonal pattern, which is similar the lattice of the triangular photonic crystal is evident. Units are in μm for the x and z and arbitrary intensity units on the y-axis.

Hexagonal patterns of the intensity peaks are evident. In a bulk sample of photopolymerizable material, cylinders of polymerized material with their symmetry axis along the y will result from this intensity profile. Cylinder size will be controlled by the intensity of the incident light and by the threshold intensity of the photopolymeric resin. The higher the intensity relative to the threshold the closer the features will be.

2.4 One Dimensional Photonic Structures formed using H-TPIP

Grating structures were produce on spin coated thin film samples of the NOA 72 and AF380 material. In the case of the thin film the structure was essentially a sinusoidal diffraction grating and was a first step towards recording planes of polymerized material in a bulk sample. Initial recordings in the thin film provided volume-grating structures with 3 μm periods and modulation depths of 50 nm at the surface [31]. To examine the diffraction properties of the gratings, diffraction spots of a red HeNe laser with a wavelength of 632.8 nm were measured and the periodicity was calculated for comparison with results from the imagery. Images of the gratings are shown in figure 2.4.1.

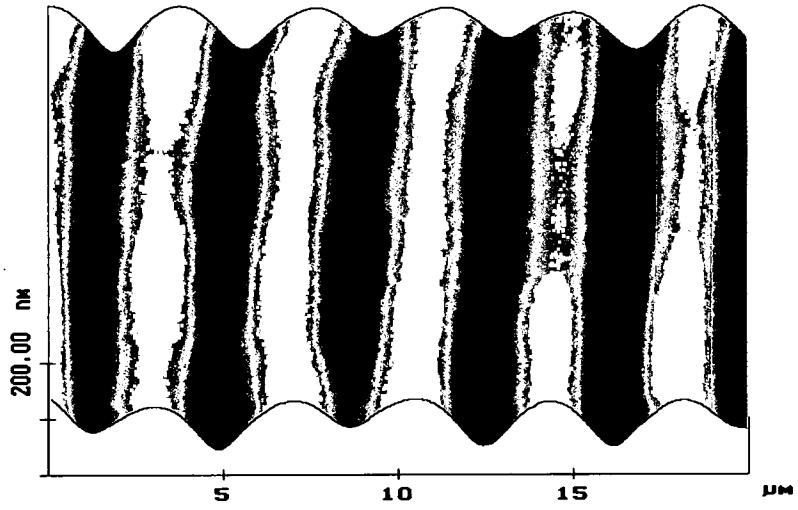

Figure 2.4.1 Grating structure produced using H-TPIP with period 3.3μm and a modulation depth of 50 nm.

Measurements of the spacing from the images indicate periods between 3 and 3.3 μm and calculated spacing from the diffraction of the HeNe gave results indicating a period of 3.5 μm [31]. A diffraction efficiency of 20% for the first order diffraction spot was measured for the HeNe.

Successful H-TPIP recording in a thin film lead to the construction of planes of polymerized material in a bulk sample. The holographic configuration was set up to provide counter propagating beams. An image of the polymerized material is shown in figures 2.4.2a and 2.4.2b. It is clear from the figures that there are planes of polymerized material. Planes close to the edge have some additional modulation on them due to Fresnel reflections from the surface of the sample holder.

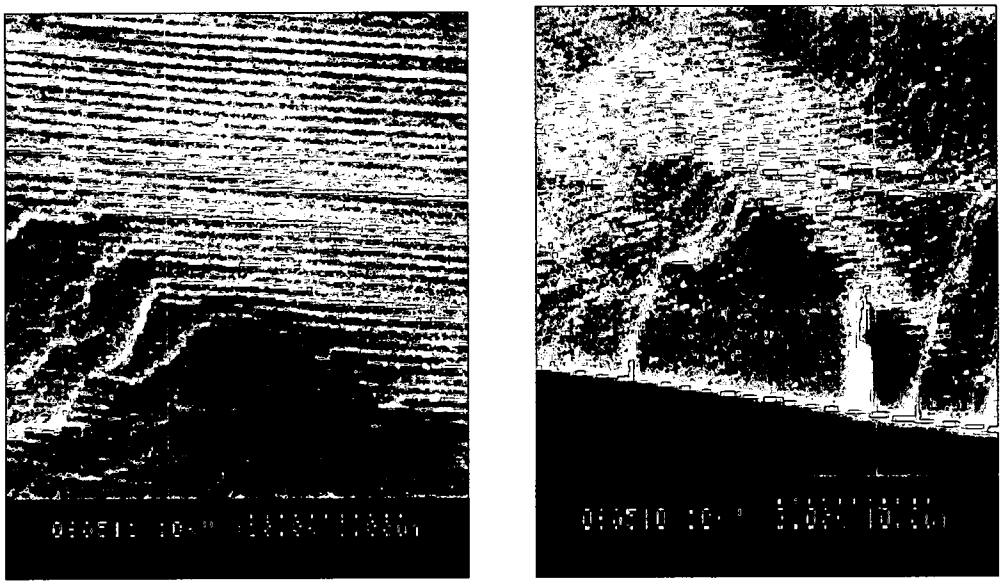

2.4.2a 2.4.2b

Figure 2.4.2. Images of photopolymerzed planes of a 1D photonic crystal. Spacing is approximately 120 nm. Figure on the right is an enlargement to illustrate the planes of polymerized material.

The image on the right is a magnification to better illustrate the polymerized planes. Planes of polymerized material are present with an approximate period of 120 to 130 nm. These values are consistent with the calculated value of 125 nm for a wavelength of 790 nm.

2.5 Band Structure Calculations and BPM for 1D Photonic Crystal

To examine the band gap properties and usefulness of the one-dimensional photonic crystal constructed above, analysis with the eigenvalue solution and BPM was performed. Essentially the photonic crystal is composed of polymerized planes with air in between them. The index of the polymerized material is approximately 1.57 [41] and the modulation period is approximately 300nm. A band structure calculation is shown in figure 2.5.1 along with the BPM results for a crystal with period, *a*, of 120 nm.

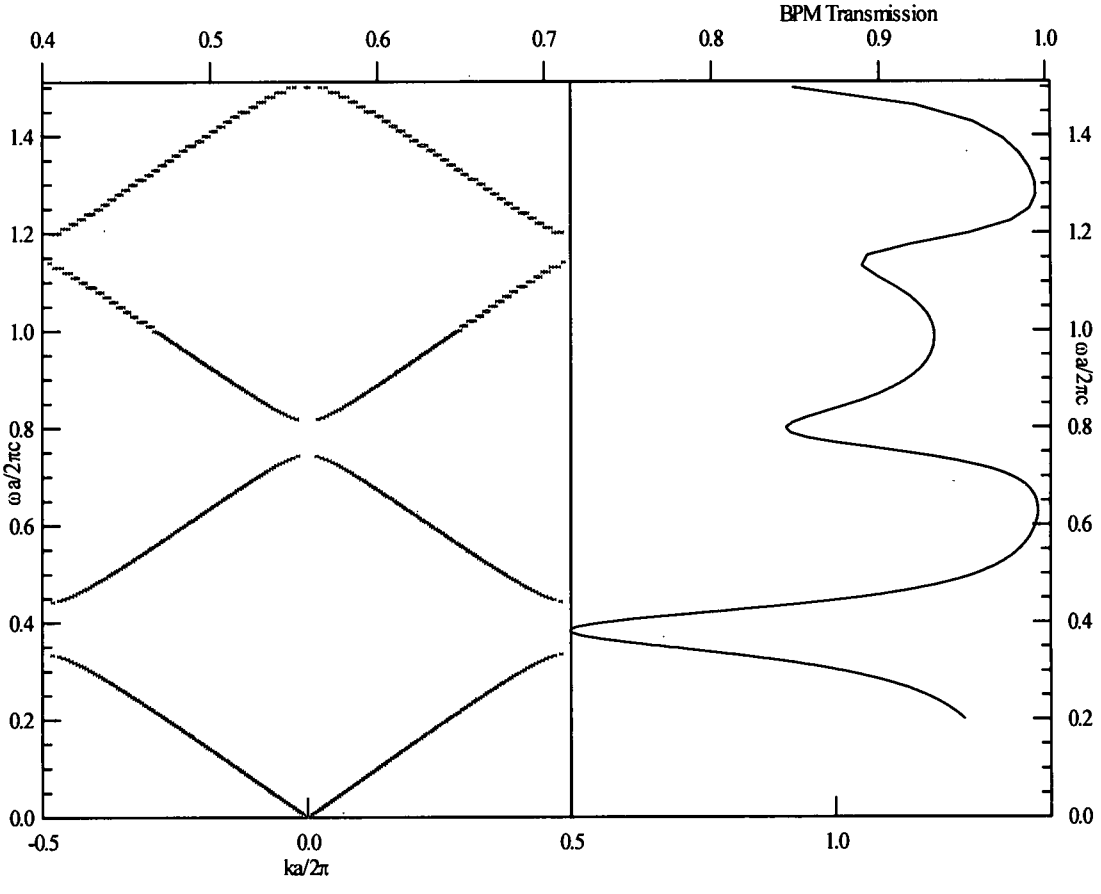

Figure 2.5.1. Eigenvalue solution and BPM results for a 1D photonic crystal with alternating regions of refractive index of 1.0 and 1.57 and a periodicity of 120nm. Eigenvalue results are on the left and the BPM results are on the right.

The lower axis is for the analytical solution and the tope axis is for the BPM transmission. Location of the transmission notches from the beam propagation method is consistent with the band gaps calculated by the analytical solution. Gaps appear between the first four bands. For the structure modeled with the BPM the wavelengths corresponding to the center of these gaps are, 325 nm, 225 nm, and 75 nm. This technique shows promise as a manufacturing method for photonic crystals that will operate in the optical wavelength region of the spectrum.

2.6 Nano Channel Glass (NCG)

Nano-Channel Glasses (NCG) are two-dimensional photonic crystals consisting of a triangular array of air channels in a glass substrate. It has been shown that Nano-Channel Glasses can be manufactured at NRL with channel sizes as small as several nanometers [42]. Channel diameters of 300 nm to 8μm are used in this experiment with the spacing ranging from 450 nm to 12 μm respectively. The spacing is approximately three times the radius of the channels resulting in the ratio of the channel radius to the spacing, *r/a*, of 0.33. Cylindrical wafers of the NCG are cut to a thickness of 300 μm and diameters of 2.5 cm. Post processing and polishing can be used to obtain wafers as thin as 30 μm.

2.7 Technique for Constructing Nano Channel Glasses

NCG samples are manufactured by means of inserting a high lead content glass rod into a glass tube and drawing the combination to a fiber [36]. These fibers

are then cut and packed, in the appropriate matrix, and redrawn in an iterative process until the desired channel size and spacing is achieved [42]. This process is illustrated in figure 2.7.1 [43].

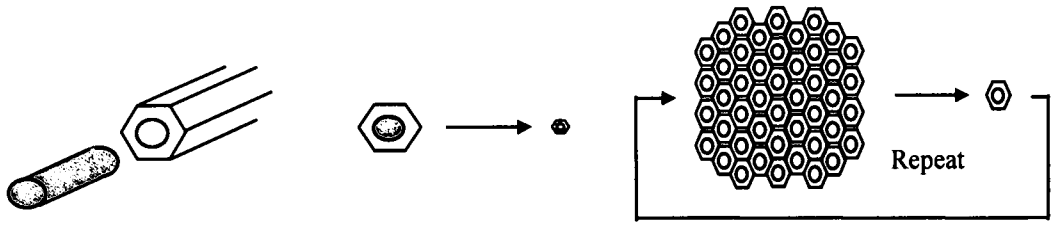

1. An etchable glass rod is inserted into inert glass tube.
2. Arrangement is drawn at elevated temperature.
3. Elements are bundled, clamped, and redrawn.

Figure 2.7.1. Illustration of the NCG manufacturing process

The glass is cut to the desired dimensions and an etching process is used to remove the high lead content glass, producing the nano-channels.

2.8 Preparation of Nano Channel Glasses

NCG samples are received from the Naval Research Laboratories (NRL) in the form of disks, each with a diameter of 2.5 cm and thickness of 300 μm to 1 mm. A polishing process is carried out to adjust the sample thickness and to give it an optical quality finish. This must be done prior to the etching process or the air filled channels will become clogged with the diamond

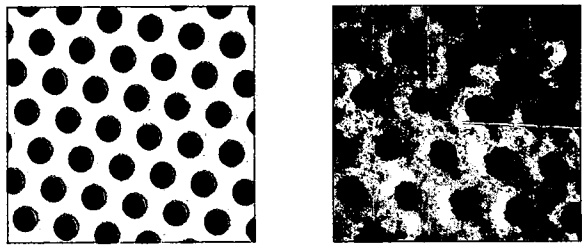

Array of 600 nm pores

Array of 15 nm pores

Figure 2.8.1. Etched Photonic Bandgap Crystals

polishing powder. Polishing of the NCG can be performed with the channels perpendicular or parallel to the polishing surface. Application of the nano channel glass dictates the orientation in which they are polished. The high lead content glass, at the channel positions, is etched with a solution of 100 mL of acetic acid and 2 drops of nitric acid. In order to etch evenly from both sides of the wafer it must be in constant free fall. This is accomplished by rotating a cuvett containing the etching solution and NCG sample. Figure 2.8.1 shows SEM pictures of two processed crystals [43].

2.9 Band Structure Calculations and BPM for NCG

Band structures for crystals with a glass matrix material of refractive index 1.6 and a channel index of 1.0, with a ratio of the radius to the spacing, *r/a*, of 0.33 are shown in figures 2.9.1 and 2.9.2. No band gaps exist for the TM case but a very small gap does appear for the TE case.

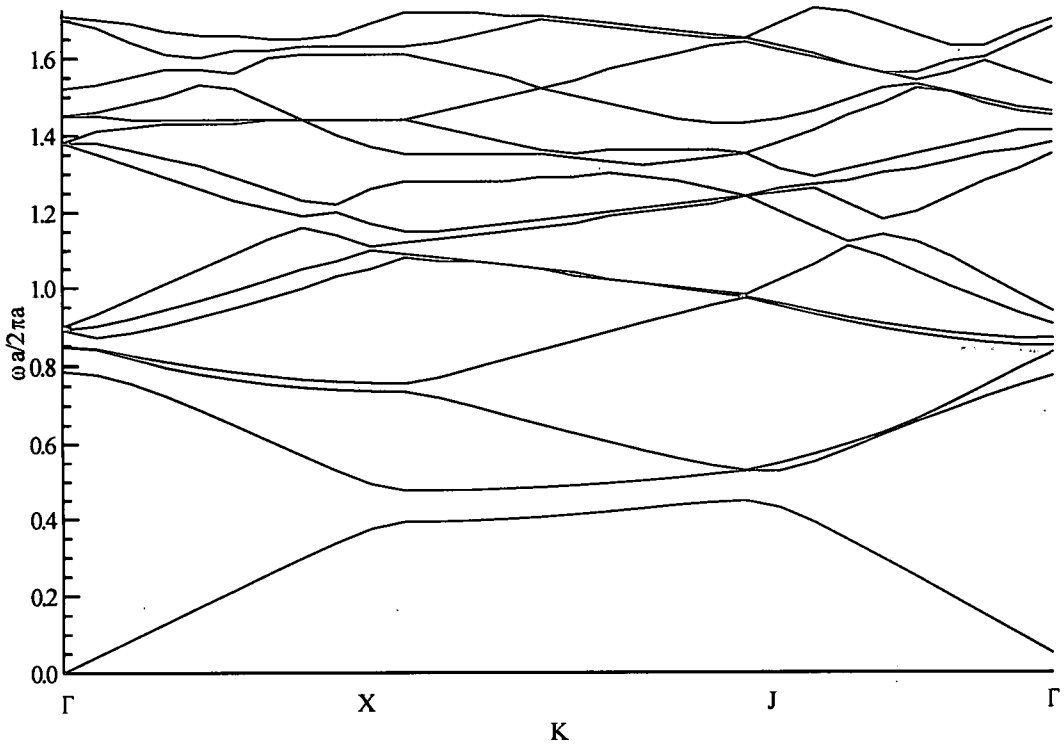

Figure 2.9.1 Eigenvalue band structure for the TE case with a channel to spacing ratio of 0.33 and an index contrast of 1.0:1.6.

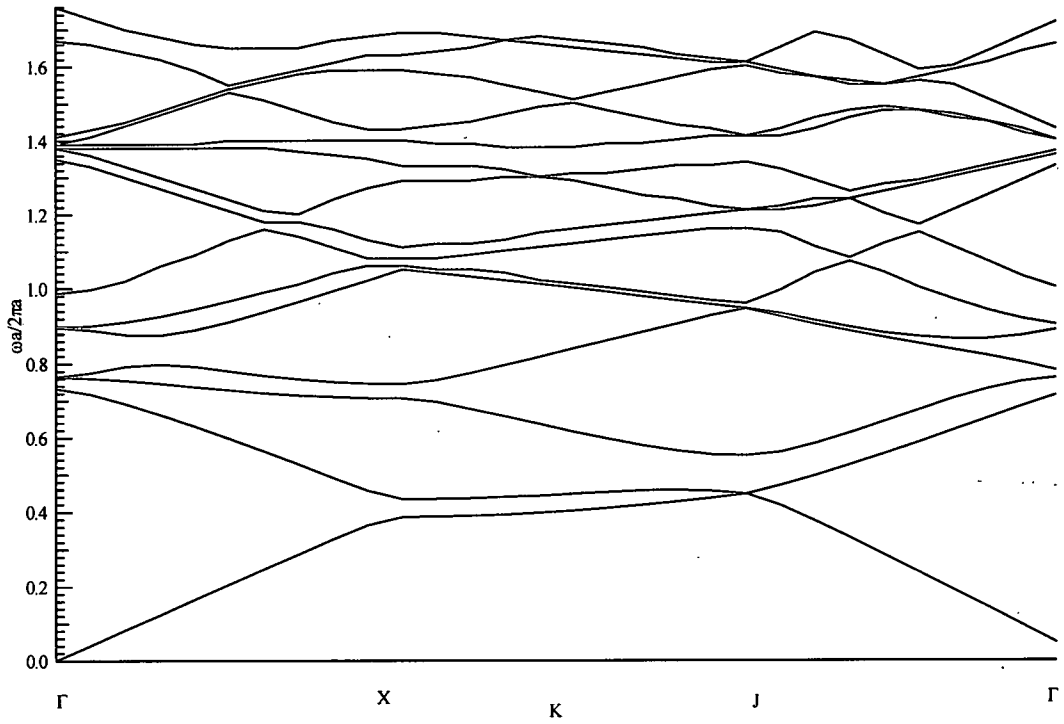

Figure 2.9.2 Eigenvalue band structure for the TM case with a channel to spacing ratio of 0.33 and an index contrast of 1.0:1.6.

This gap is centered at the wavelength $a/0.46$. For the case of a 450 nm spacing the gap would be centered around 650 nm and for a 1 μm spacing the center wavelength would be around 2.17 μm.

To further understand the nature of the NCG a BPM analysis was performed. A sample with a channel size of 300 nm and a separation of 450 nm was chosen with propagation along the Γ-J direction. Again, due to the propagation direction only the band structure along this vector is of interest. Figures 2.9.3 and 2.9.4 illustrate the band structure from the eigenvalue solution for TE and TM case in the Γ-J direction along with the BPM result. Both band structures show band gaps but they do not overlap. A fairly large bandgap arises between the first and second bands for the TE case over a wavelength range of 865 nm to 1.02 μm, for this sample. Another very small gap is present for the TM case and is centered at 535 nm. Two very small gaps exist for the TE case and are centered at 584 nm and 384 nm.

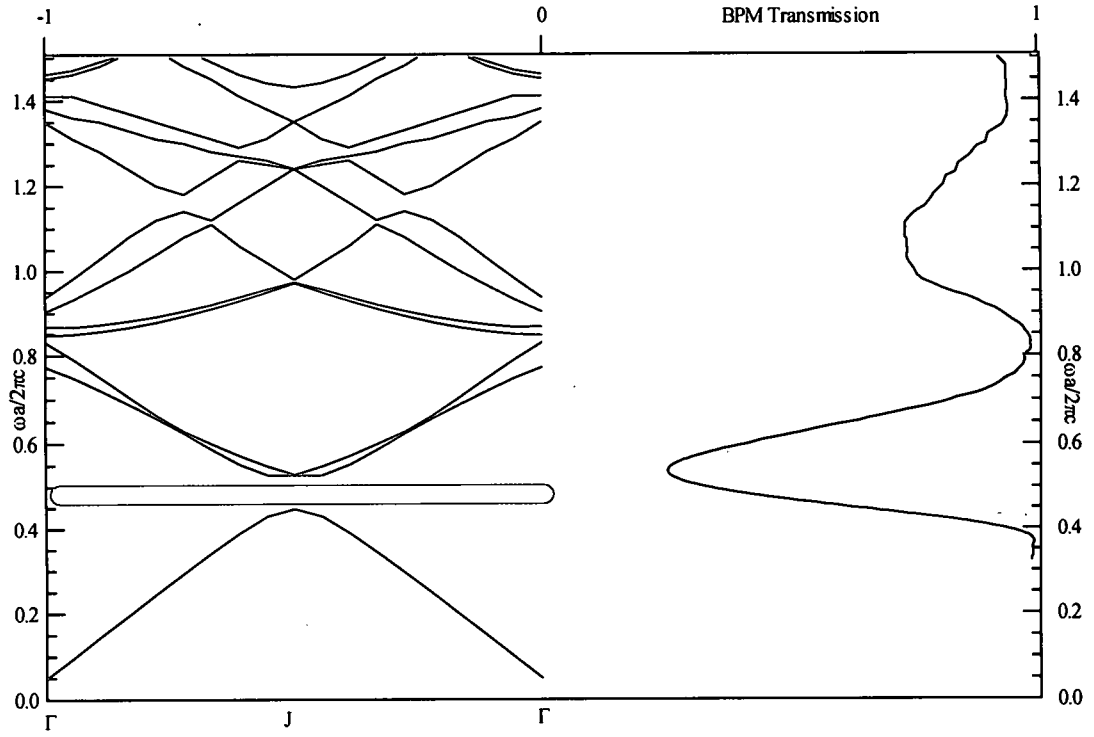

Figure 2.9.3. TE case with Eigenvalue solution and BPM for propagation limited to the Γ-J direction. The eigenvalue solution is on the left and the BPM results are on the right.

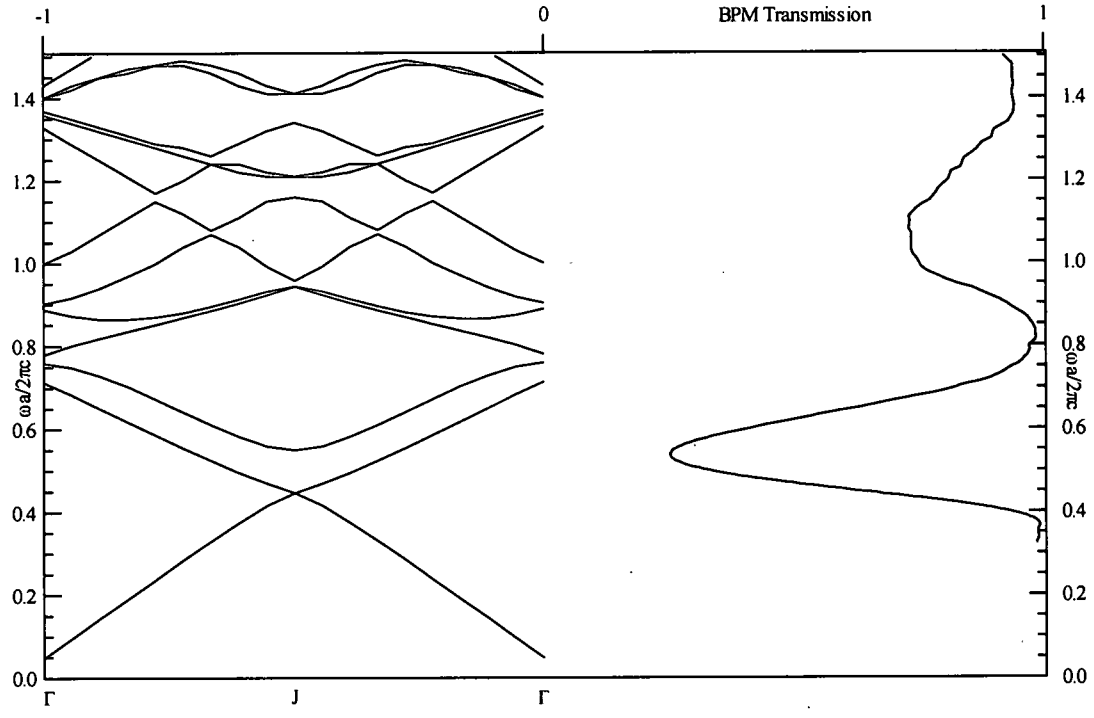

Figure 2.9.4. TM case with Eigenvalue solution and BPM for propagation limited to the Γ-J direction. The eigenvalue solution is on the left and the BPM results are on the right.

BPM results show a large transmission valley at the location of the large band gap for the TE case on figure 2.9.3. This valley is centered at 850 nm for the channel spacing of 450 nm. The small dip in the transmission at the left of the plot is centered at 425 nm and is possibly a harmonic of the large valley or a result of the small band gaps for the TM and TE case which are centered at 385 nm and 535 nm respectively. It is apparent that the transmission valleys are not limited to the wavelength regions dictated by the band structure plots. This is a result of resolution limits in the BPM program and imperfections in modeling the photonic crystal structure.

Due to the fact that the available crystals do not show large band gaps limits their use as stand alone photonic crystals. NRL has the ability to construct crystals with closer spacing and smaller channel diameters, increasing the photonic band gap nature of the nano channel glasses. Incorporation of other materials inside the channels can possibly enhance the bandgap nature of the NCG as well. Other applications for these types of structures have been examined including nano channel patterning [44] and optical switching and waveguiding, which are applications examined in a latter section.

CHAPTER 3

Dynamic Photonic Band Gap Structures

It is of interest to examine the possibility of a dynamic system in which the band structure of a photonic crystal changes with some arbitrary input. An approach to a dynamic photonic band gap structure lies in the use of liquid crystal in conjunction with a photonic crystal. Liquid crystals (LC) have been incorporated into many devices including liquid crystal displays and optical switches [45,46]. Advancements in the field of telecommunications and the advent of optical computing will necessitate the ability to switch information very rapidly. Incorporation of LC into one and two-dimensional photonic band gap materials can provide a structure with this ability. It is possible to include liquid crystal droplets into a periodic matrix such as a polymer dispersed liquid crystal (PDLC) [16], the planes of a photopolymerized one-dimensional photonic crystal, or the channels of a two dimensional photonic crystal. In these structures the liquid crystal can be switched in order to index match to the surrounding material or index mismatch to the surrounding material, thus diffracting radiation or producing a photonic band gap. Waveguiding can also occur in the channels of a

two-dimensional photonic crystal by incorporating a material with a higher refractive index than that of the matrix material. By filling the channels of a NCG sample with LC, the waveguiding properties of the system can be altered by switching the orientation of the LC and therefore the index contrast between the LC and the glass matrix.

3.1 Liquid Crystal

Liquid crystal is a material state in which the optical properties, such as the refractive index and dielectric constant, will depend on an applied electric field, the temperature, and the pressure of the material [45,46]. Light propagating through LC will experience anisotropic refractive indices, which are dependent upon the orientation of the liquid crystal molecules with respect to the polarization of the propagating beam. In essence liquid crystal molecules are birefringent materials with ordinary and extraordinary indices of refraction, n_o and n_e respectively. Three types of liquid crystals have been discovered so far and include thermotropic, lyotropic, and polymeric [45,46]. Thermotropic liquid crystals have been studied extensively and many applications have come to fruition with this type of material. Liquid crystal displays (LCD) are the most widely know examples. Three possible phases exist for thermotropic liquid crystals and include nematic, cholestaric, and smectic [45,46]. Nematic thermotropic LC will be used in the following experiments. In the nematic phase the molecules are approximately in the same orientation but are not ordered in their positions [45,46]. A symmetry axis along the molecular orientation is called the director and can be reoriented by

applying an electric field [45,46]. Doing so alters the refractive index for a specified propagation direction and polarization of light incident on the material. Nematic E7 liquid crystal is used in these experiments and is uniaxial with ordinary and extraordinary indices of refraction, n_o and n_e of 1.53 and 1.76, respectively. Applying a voltage will essentially orient all of the liquid crystal molecules such that their directors are parallel to the applied field. When no field is applied the LC molecules will be randomly oriented and the refractive index experienced by an incident beam will be in between n_o and n_e.

3.2 Recording of a Transmission Type PDLC Grating using H-TPIP

Polymer dispersed liquid crystal structures are a periodic medium with a dynamic dielectric which offers the ability to rapidly switch optical beams. Liquid crystal droplets contained in the PDLC are randomly oriented and exhibit an average index of refraction somewhere between the n_o and n_e refractive indices. If this index and the index of the polymer substrate are mismatched an index grating is present. Illumination of the grating with coherent light will result in diffraction of the beam. Reorientation of the LC in the PDLC by applying a voltage will alter the refractive index mismatch between the LC and polymer and it is possible to alter the index such the material will become transparent to the illuminating beam.

Several techniques exist for the construction of PDLC structures including one and two-photon induced photopolymerization. In this report the focus will be on the two-photon process due to the skewed polymerization rate. As

discussed in chapter two the rate of polymerization is slower outside the regions of high intensity in the two-photon process. The slower rate of polymerization will influence the size and definition of the liquid crystal domains due to the fact that the LC droplets will have more time to diffuse to the monomer regions before they are trapped in the polymer [34]. This not only improves on the definition of the LC domains but also reduces cross-linking between the polymerized regions through the LC. Bis(diphenylamino) diphenyl hexatriene was selected as the two-photon absorber and has a cross section of 1.55×10^{-20} cm^4/GW [34]. Formulation of the photopolymer was accomplished using 0.5% of this amine, a free radical polymerizable monomer dipentaerythritol pentacrylate (DPHPA) 57%, N-vinyl pyrolidinone (NVP) 10%, and nematic liquid crystal E7 32% [34]. This material was sandwiched between two ITO coated glass slides with a separation of approximately 8 μm.

A neutral density filter was used to reduce the energy at the sample to 120 μJ and 150 μJ for the object and reference beams respectively. The energy at the recording plane was such that the exposure times were 60seconds. Electron microscopy was performed on the PDLC structures with a Low Voltage Scanning Electron Microscope (LVSEM). A Nikon Optiphoto microscope, in transmission, was used to perform optical microscopy. LVSEM images of the transmission type PDLC structure is illustrated in figures 3.2.1 and 3.2.2. Image 3.2.3 is a magnification of figure 3.2.1 to illustrate the liquid crystal droplets encapsulated in the polymer.

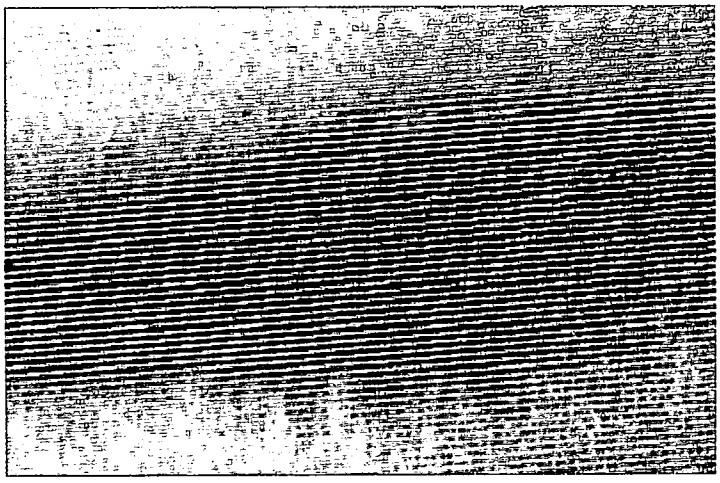

Figure 3.2.1. LVSEM image of PDLC formed using H-TPIP

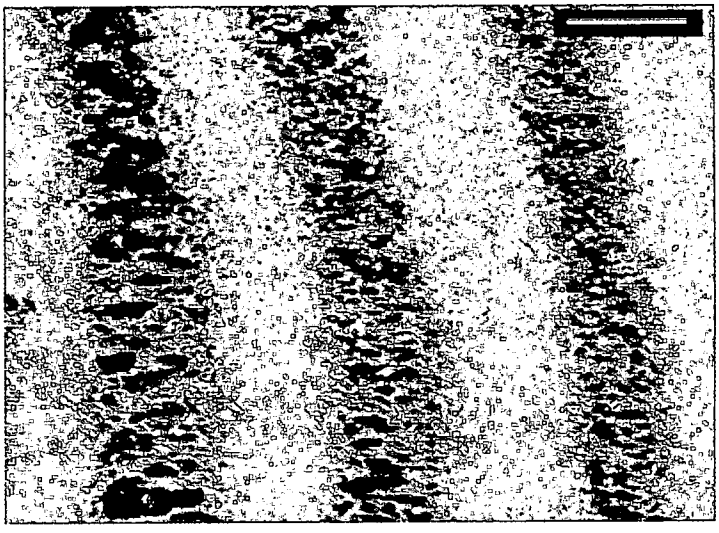

Figure 3.2.2. LVSEM image of PDLC formed using H-TPIP.

It is clear in these images that a bulk grating was formed with domains of LC dispersed by regions of polymer. Domains of LC are periodic with a separation of approximately 3-μm and the thickness is approximately 8-μm with 25-30% of the periodicity composed of LC regions [34].

Modulation of an optical beam was observed using a He-Ne laser and a 2 kHz square wave electric field applied to the ITO coated slides. Applying a voltage to the plates reduces the diffraction by decreasing the mismatch between the refractive indices of the LC and the polymer. Observation of the 0^{th} order diffraction spot shows an increase in intensity, with an applied voltage, while the 1^{st} order diffraction spot shows a decrease in intensity. Figure 3.2.3 shows the intensity of the 1^{st} order diffraction spot as a function of voltage [47].

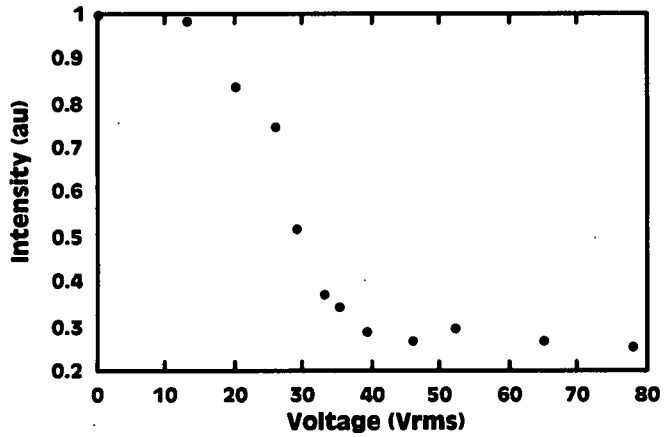

Figure 3.2.3. Switching curve for PDLC. Intensity of the 1^{st} order diffraction spot.

The intensity of the second order diffraction spot is minimized after a voltage of 40 V_{rms}, is applied. At this voltage and with a thickness of 8 μm, the switching field is 5 V/μm. Voltages of 4 V/μm have been achieved with conventional photolithography techniques, but only after years if refinement. With this two-photon technique, on the first try, a comparable switching voltage has been

achieved. With some refinement, PDLCs constructed with this method will exhibit switching voltages well below the current values.

3.3 One Dimensional Photonic Crystal Incorporating Liquid Crystal

Utilizing the techniques described in chapter 2 and the photopolymerizable system described above it is possible to incorporate liquid crystal into a one-dimensional photonic crystal structure. This process will produce a dynamic photonic crystal, which can act as a filter or mirror. A sample of the polymerizable system above was sandwiched between two ITO coated plates with an 8 μm spacer. Planes of liquid crystal droplets were formed in a bulk sample with a periodicity of approximately 120 to 130 nm. Again the periodicity is close to the predicted value of 125 nm. This translates to regions of LC and polymer each with lengths of 60 to 65 nm. Again the ordinary and extraordinary indices of refraction, n_o and n_e, of the liquid crystal are 1.53 and 1.75 respectively [41]. The refractive index for the polymerized material ranges from approximately 1.53 to 1.56 [41]. Applying a dc electric field to the sample, perpendicular to the planes of polymerization, orients the LC such that a beam propagating normal to the planes will see the ordinary index of refraction. In this case the indices of the two materials, the LC and the polymer, are approximately matched and the transmission, aside from loss, is unity. Without any field applied to the sample the liquid crystal is randomly oriented and light propagating normal to the planes will see an index in the LC that is an average of n_o and n_e. An index

contrast of approximately 1.53:1.64 is present as a result of the random orientation of the LC and a band gap will result form this index contrast.

The switching and filtering properties of the sample were examined by applying a voltage to the ITO coated slides. Transmission of an unpolarized white light source through the sample was observed with the use of a spectrometer. The spectrum of the output was measured as a function of the applied voltage and is illustrated in figure 3.3.1 for applied voltages of 1.20, 0.80, 0.40, and 0 volts rms [48].

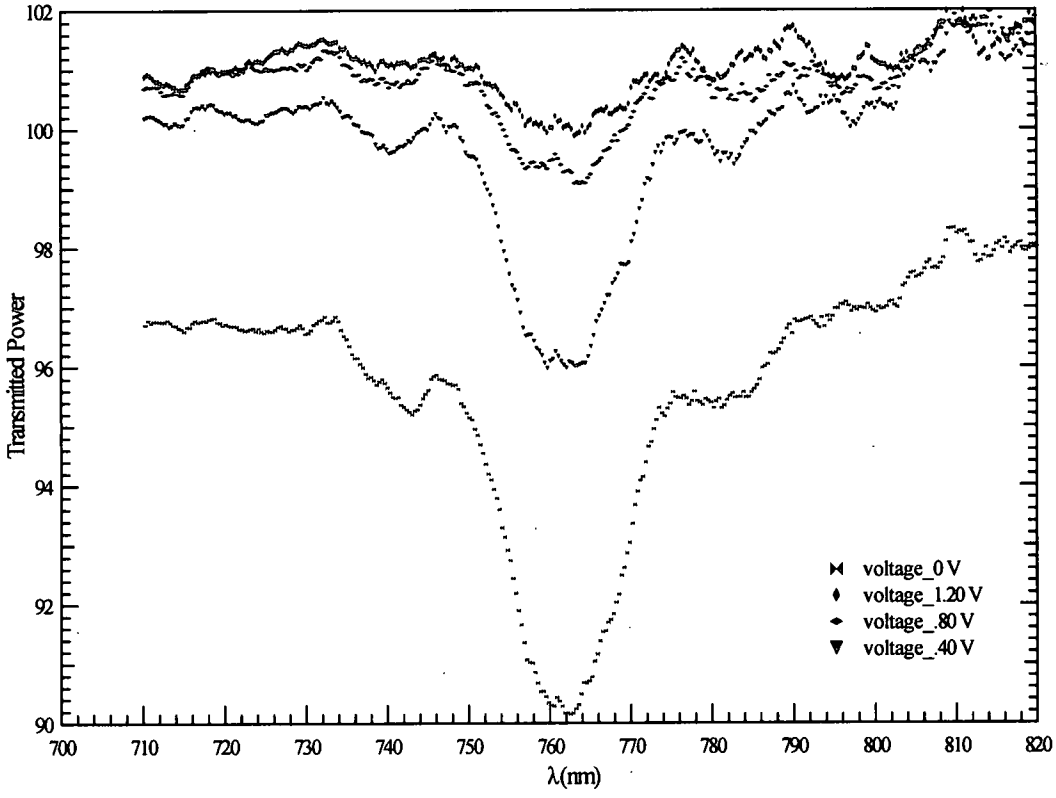

Figure 3.3.1. Transmitted spectrum for a 1D photonic crystal incorporating LC. Spectrum shows the dependence on the applied voltage.

A notch appears which is centered at 760 nm. As expected, the transmission increases as the voltage is increased. This is a result of the orientation of the LC

such that the indices of the LC and the polymer are matched for a beam propagating normal to the planes. Scattering from the random orientation of the liquid crystal causes the power level to be decreased across the entire spectrum when little or no voltage is applied.

BPM code for the 1D photonic crystal was employed to further examine the transmission properties of the crystal and to verify the solution with results from experiment. In figure 3.3.2 the spectrum for voltages applied to the crystal of 1.20 V rms and 0 V rms are shown along with the output of the BPM code. The experimental results were normalized to give more insight into the effect on the transmission of applying a voltage across the sample. In the BPM code, for the case when no voltage is applied, the refractive indices for the polymer and LC were 1.53 and 1.64 respectively. Each region was set to 60 nm and the field was propagated through 50 layers of the photonic crystal, translating to 3 μm. The same BPM was performed with a 120 V rms voltage applied to the ITO coated slides. It is assumed that the liquid crystal does not completely orient itself with the applied field and the field does not propagate completely normal to the plans. Therefore, in the BPM code when the applied voltage is 1.20 V, the indices of refraction for the polymer and the LC are assumed to be approximately 1.53 and 1.54 respectively. These results are plotted in the figure as well.

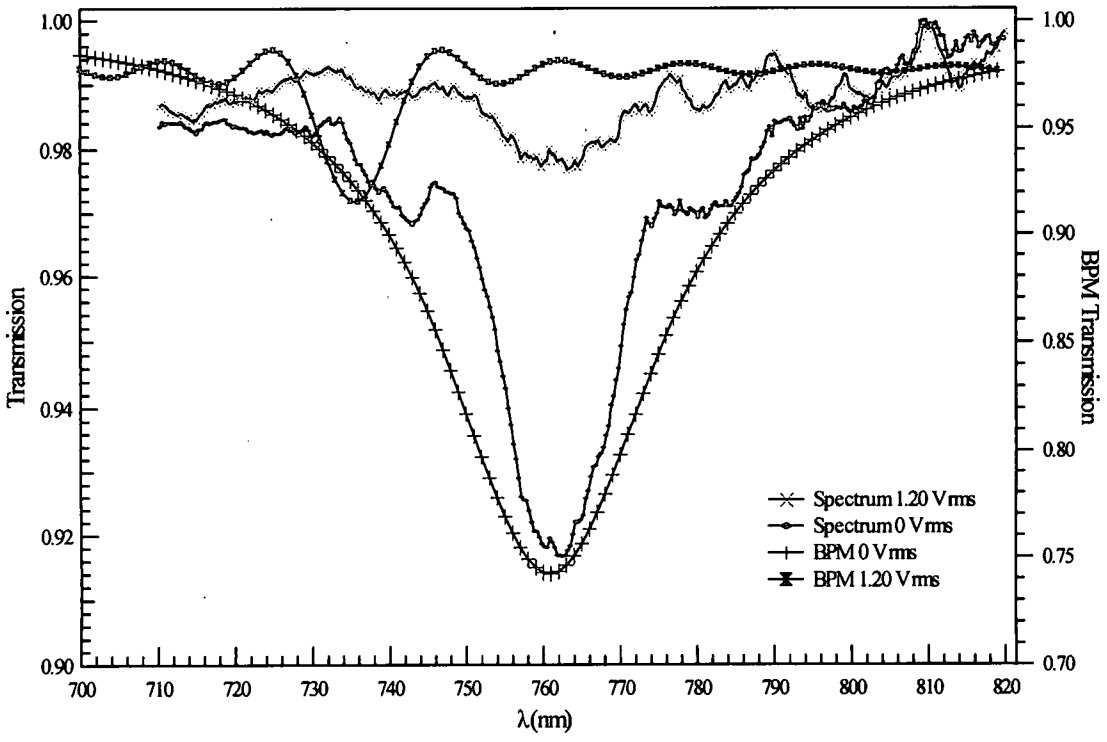

Figure 3.3.2. Spectrum and BPM for applied voltages of 1.20 V rms and 0 V rms. Notch from the BPM is consistent with that of experiment

In the experiment the number of planes is approximately 66. In addition, the scattering effects found in the experiment are not taken into account by the BPM code. As a result the value of the transmission given by the BPM output is not very meaningful but the location of the notch is valid. A notch is present on the BPM output at approximately 760 nm, which is consistent with the experimental results. It is interesting to note that the BPM code shows a shift in the notch when the indices are altered by applying a 1.20 V field, shown in figure 3.2.5. This is a result of the change in path length and a change in the localization of the field power, which was discussed in section 1.2. The experimental results do not show this shift and may be a result of the broad band nature of the

recording beams or experimental error. A structure such as this can provide a dynamic filter or optical switch as a result of the ability to alter the transmission notch by simply applying a voltage across the device.

3.4 Incorporation of Liquid Crystal into Nano Channel Glasses

Nano channel glass samples were prepared and filled with E7 nematic liquid crystal to examine the application of these structures as optical switches. It is expected that the LC filled channels will act as waveguides when the appropriate waveguiding conditions are met and the waveguiding properties will be affected by applying a voltage across the sample. A waveguide consists of a core with an index of refraction, which is higher than the surrounding material. Generally, a glass core is surrounded by a glass cladding, which has a slightly lower index. In the case of the liquid crystal inside the channels of the NCG the waveguiding conditions are meet due to the fact that the ordinary index of refraction is 1.53 and the index of the glass is approximately 1.45. It was initially our intention to switch between the extraordinary index, and the ordinary index to enhance or prohibit waveguiding. This could not be achieved because the lowest index of the LC is higher than that of the surrounding glass. However, it is possible to enhance containment of a propagating field in the LC filled channels in an on state, with an applied voltage, due to the fact that the LC molecules are uniformly oriented, as opposed to the random orientation in the off state. Scattering is a result of the random orientation of the LC molecules, causing light to propagate away from the waveguide formed by the liquid crystal and the nano

channel glass. The following is the experimental results showing that light containment in LC filled channels of a NCG sample will be enhanced by the application of an electric field parallel to the channels.

A sample of the NCG with 6 μm channels and a thickness of 75 μm was prepared and filled with E7 nematic liquid crystal having ordinary and extraordinary refractive indices, n_o and n_e, of 1.53 and 1.76 respectively. The sample was then sandwiched between two ITO coated slides positioned such that they closed off the ends of the channels. To examine the effects of switching the voltage a 2 kHz square wave electric field was applied to the ITO plates to modulate a HeNe beam. The laser was incident normal to the plane of the ITO coated plates.

To understand the switching properties of the system the output of two LC filled channels were measured with a pin diode photo-detector, relative to several applied voltages. A plot of the power at the photo-detector verses the applied voltage is shown in figure 3.4.1. Plots of a central channel and an adjacent channel are shown in the figure [48].

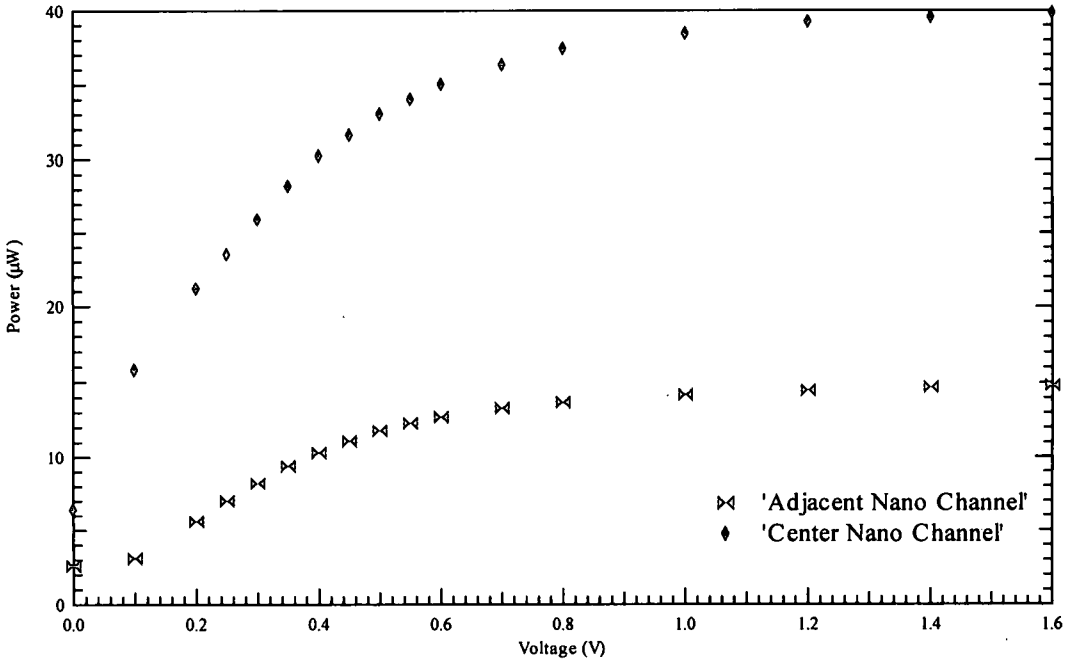

Figure 3.4.1. Switching curve a central and adjacent channel of HeNe laser through a NCG sample filed with E7 nematic LC.

The HeNe was focused into the sample with a microscope objective and the output was imaged onto the detector via a lens. It is apparent that both channels have an increase in transmission with an increase in the applied voltage. At approximately 0.8 V the plots begin to level off, implying that LC directors are reaching their full orientation along the applied field. The plot implies that the HeNe is more confined to the channels with the voltage on and the LC uniformly oriented than with the voltage off.

A CCD camera was also employed to image the crystal as the HeNe was modulated. Images of the LC filled crystal with the HeNe incident upon it is shown in figures 3.4.2 through 3.4.6. The voltage was modulated between 0 V and 1.30 V rms [48].

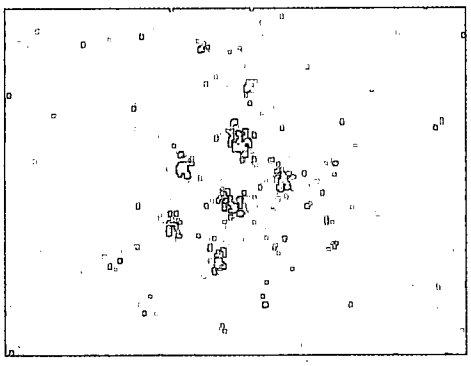

Figure 3.4.2. Image of HeNe propagating through NCG filled with LC. Applied voltage is 0 V.

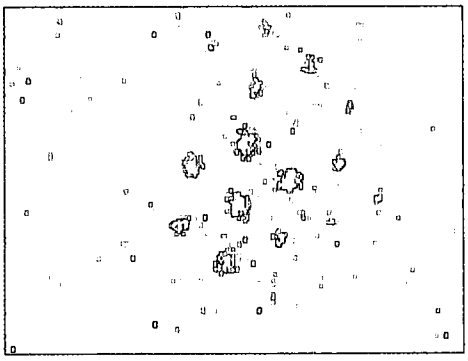

Figure 3.4.3. Image of HeNe propagating through NCG filled with LC. Applied voltage is 0.29 V.

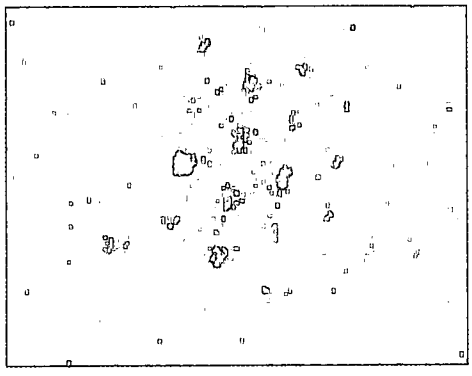

Figure 3.4.4. Image of HeNe propagating through NCG filled with LC. Applied voltage is 0.35 V.

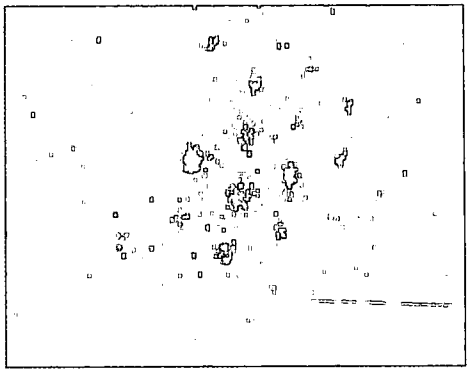

Figure 3.4.5. Image of HeNe propagating through NCG filled with LC. Applied voltage is 0.52 V.

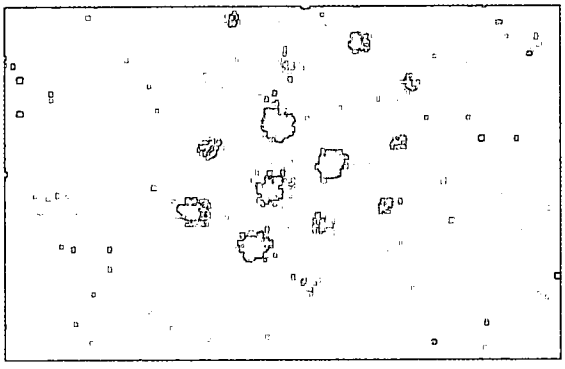

Figure 3.4.6. Image of HeNe propagating through NCG filled with LC. Applied voltage is 1.30 V.

Again it is shown that the intensity output of the channels is increased, with an increase in the input voltage.

It would be of interest to design a similar system with a NCG sample of a slightly higher refractive index. Applying a field parallel or perpendicular to the channels, and the direction of light propagation, will offer the ability to switch between waveguiding and inhibition of waveguiding. In this case, individual channels could be addressed, similar to addressing micro-mirror arrays, in a multiplexing arrangement to provide high-speed communication links between multiple channels. This could be accomplished by positioning an optical fiber of a communications link such that it is aligned with a single channel of the crystal, like a micro-channel plate. The LC in a particular channel could be addressed to switch light in and out of the fiber.

CHAPTER 4

NCG as Hosts for Laser and Detector Materials

Low-lying manifolds of rare earth ions have transitions in the mid infrared and, provided there is limited multiphonon quenching, have the potential to act as mid infrared sources of radiation due to their ground state splitting. Unfortunately, high multiphonon quenching in conventional oxide and fluoride host materials deactivates these radiative transitions [49]. Doping rare earth ions into a low phonon host, materials with a low phonon density of states, eliminates multiphonon quenching and enhances radiative emission [49-54]. Growth of these hygroscopic materials inside a two-dimensional photonic crystal can provide isolation from the environment and it is believed that some of the IR emission and absorption transitions of the rare earth low phonon crystals will be affected by growing these materials inside these structures [55,56]. In this work the focus will be on growth of optical quality crystals inside the nano-channel glasses for the purpose of isolating these materials from the environment while the band gap nature of the photonic crystals is a secondary issue.

4.1 Rare Earth Doped Low Phonon Crystals

Provided there is limited multiphonon quenching, rare earth ions, specifically erbium, have the potential to act as mid infrared sources of radiation due to their ground state splitting. Transitions in the IR, in the 3.5 μm - 5 μm spectral range, are useful due to their spectral positions within an atmospheric window. High multiphonon quenching in conventional oxide and fluoride host materials deactivates these radiative transitions [49-51]. Doping rare earth ions into a low phonon host, materials with a low phonon density of states, eliminates multiphonon quenching and enhances radiative emission. These rare earth low phonon crystals have been shown to emit in the mid-IR region at room temperature [49-51].

Detection of IR radiation is of interest as well and is examined in the trivalent terbium ion. Low-lying transitions in Tb^{+3}, which are not thermally exited at room temperature, will absorb in the 8 μm to 12 μm wavelength regime. Using a broadband laser in the visible, it is believed, an excited state produced by an absorbed IR photon can be pumped to a high energy state which will then decay, emitting a visible photon. Figure 4.1.1 illustrates the energy transitions of Tb^{+3}.

Erbium doped chlorides, in trivalent form, have shown the necessary quantum efficiency and energy storage lifetimes for consideration as mid-IR emitters [49-51,57,58]. Figure 4.1.1 shows the energy level diagram for the pertinent transitions in Er^{+3}. Four emission transitions are apparent, namely the $^4F_{9/2} \rightarrow {}^4I_{9/2}$, $^4I_{9/2} \rightarrow {}^4I_{11/2}$, $^4I_{11/2} \rightarrow {}^4I_{13/2}$, $^4I_{13/2} \rightarrow {}^4I_{15/2}$. Due to the absence of multiphonon

decay between manifolds, as well as any apparent energy transfer, cascade lasing may be possible [49].

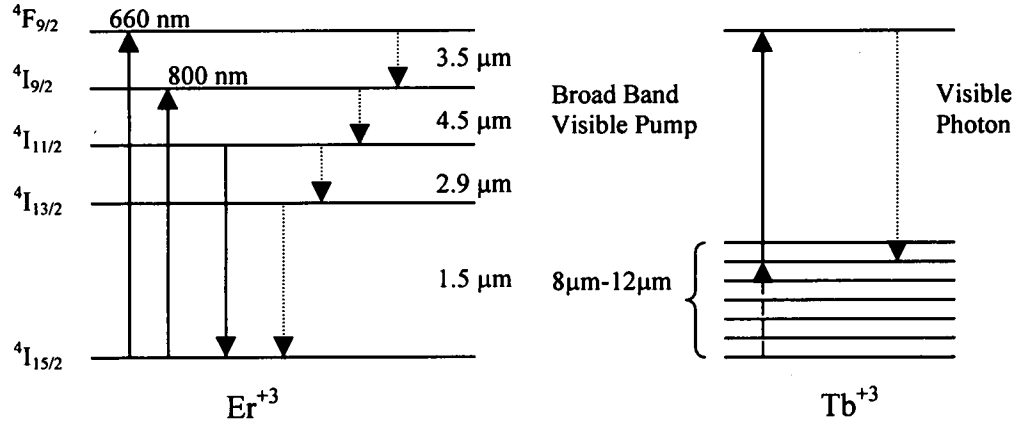

Figure 4.1.1. Energy level diagram for Er^{+3} and Tb^{+3}. The solid lines are the pump transitions and the dotted lines are the radiative transitions and the dashed lines are the detected photon in the Tb^{+3}.

Crystals such as $LaCl_3$ and $GdCl_3$ provide a low phonon host for the rare earth ions but have the disadvantage of being extremely hygroscopic. Keeping such materials isolated from the environment posses difficulties such as dealing with toxic index matching fluids. A solution to this problem is to grow these hosts inside a nano channel glass host.

4.2 Crystal Growth

Growths of single crystal structures of rare earth doped lanthanides in bulk form and inside the NCG are carried out using an adaptation of the Bridgman-Stockbarger method [59]. Single crystal growths, in conical shapes, measuring 0.75

cm at the base and 1.0 cm in height as well as single crystal growths inside NCG with 6 μm channels and thickness' of 100 μm to 300 μm have been accomplished.

The Bridgman-Stockbarger crystal growth apparatus, illustrated in figure 4.2.1, is constructed with a vertical three-zone furnace and a vertical translation stage. Growths are controlled entirely from a PC, using LabView instrumentation software, which is hardware interfaced to each furnace controller and the translation stage controller. A Yokogawa UP550 controls each zone of the furnace and can support temperatures ranging from room temperature to 1200. A Deadal 500000ET translation stage is controlled with a Zeta 6104 Parker Compumotor controller with a PC based interface.

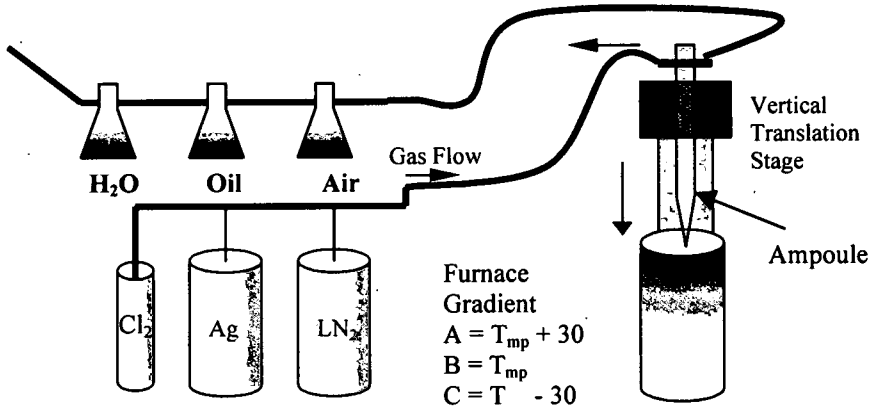

Figure 4.2.1 Crystal Growth Apparatus.

Growths are performed over a linear temperature gradient, centered at the melting point (mp) of the lanthanide, with temperatures ranging from mp-30°C to mp+30°C, over a distance of 10 cm [60]. Higher temperatures are at the top of the gradient. A low OH quartz ampoule, tapered at one end to facilitate self-seeding and containing the doped lanthanide in powder form, is lowered through the

temperature gradient. As the material is lowered through the furnace it melts in the upper portion of the gradient. When the molten lanthanide passes through the recrystalization point of the gradient a seed crystal forms at the tip of the ampoule. The crystal grows from the seed while translating through the furnace. Due to the hygroscopic nature of the material growths are performed under a chlorine gas, preventing oxychloride formation in the sample. Translation of the sample through the gradient ranges in velocity from 0.5 mm/hr to 1 mm/hr and typical growths take approximately 7 to 14 days [60]. An additional period of 24 hours is needed at the end of the growth to allow the sample to cool down to prevent stress fractures in the sample.

Each low OH quartz ampoule is used in conjunction with a glass gas flow interface with the two components connected via a Teflon coupler. This Teflon coupling device is a hollow cylinder, with external o-rings, which fits inside the ampoule and the gas flow interface. Gas flow between the two components through the hollow cylinder is allowed while the exchange of gasses to and from the atmosphere is prevented. In addition, a steel compression fitting slides over the Teflon coupler and ensures a proper seal when placing the ampoule combination under vacuum.

Quality growths really heavily on the rate of temperature change that the material experiences over the growth period. In order to control this, knowledge of the exact temperatures of the furnace zones is required. A LabView program was written which is interfaced to an 85-cm Type K thermocouple to measure the furnace temperature. In order to map the gradient under similar conditions to

those of the crystal growth, the thermocouple is placed inside an ampoule with the tip at the same position as the crystal growth material. A plot of the temperature and position is produced while lowering the thermocouple through the gradient in 0.5-cm and the three zones of the furnace are adjusted in temperature until the desired gradient is reached.

Contamination of the growth material is a common problem resulting in the growth of polycrystalline structure. HCL and Acetone are used to remove any oxides from the glass walls and to dissolve any other contaminates in the ampoule. A propane torch is also used to dry the ampoule of acetone and to remove any additional moisture. In order to ensure that the ampoule is completely absent of oxides, using the furnace, it is baked out under vacuum at 200°C for approximately 6 hours. Very low vacuum pressures are desired and generally the ampoule can be pulled down to approximately 10 milliTorr, although pressures lower than this are desired. Only clean and dry ampoules are used for the crystal growths.

A glove box, with a constant flow of dry N_2, is employed for the transfer of the material from its storage container to the ampoule. Approximately 0.5-1.0 grams of the doped lanthanide is used for each growth. The powder lanthanide is baked out under vacuum to remove any moisture from the material and the glass.

Improper seeding of the crystal also results in polycrystaline growths. To prevent this, prior to flooding the ampoule with Cl_2, the material is melted under vacuum This prohibits any gas from being captured at the tip of the ampoule under the molten sample, which impedes self-seeding.

Growth of the REDLP crystals inside the NCG is basically the same as that described above except for the accommodation of mounting the crystal inside the growth ampoule, which is shown in figure 4.2.2. Material is loaded on top of the NCG sample resting on the ledge at the lower end of the ampoule. This small ampoule is placed inside the large ampoule for the growth. As the powder melts it flows around and through the NCG and the crystal grows through the channels as the melt is lowered through the gradient.

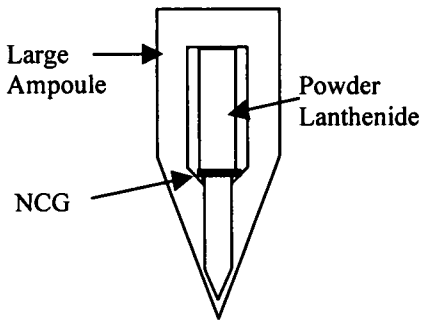

Figure 4.2.2. Ampoule for growth inside the NCG.

4.3 Crystal Growth Results

Preliminary crystal growth of Tb^{+3}:$GdCl_3$ inside a nanochannel glass having a channel size of 800 nm is shown in Figure 4.3.1 [47]. This growth was uncontrolled and was a test to see if the molten material would wick into the channels. Although this was not a controlled growth, and much of it is polycrystalline, some regions do show single crystal structure as evidenced along the cleavage plane.


Figure 4.3.1 SEM image of preliminary crystal growth of $Tb^{+3}GdCl_3$ in the PBG crystal.

Controlled growths of $GdCl_3$ inside 6 μm channels are shown in Figure 4.3.2. Single crystal areas of

Figure 4.3.2a are apparent as uniform dark areas. The nonuniform areas that are a lighter shade are polycrystalline structures or damaged single crystal, due to moisture absorption during the processing for SEM. Dark shadows around the single crystal growth in Figure 4.3.2b indicate different thermal expansion properties between the two materials, which caused the crystal to expand out of the channels of the nano-channel glass.

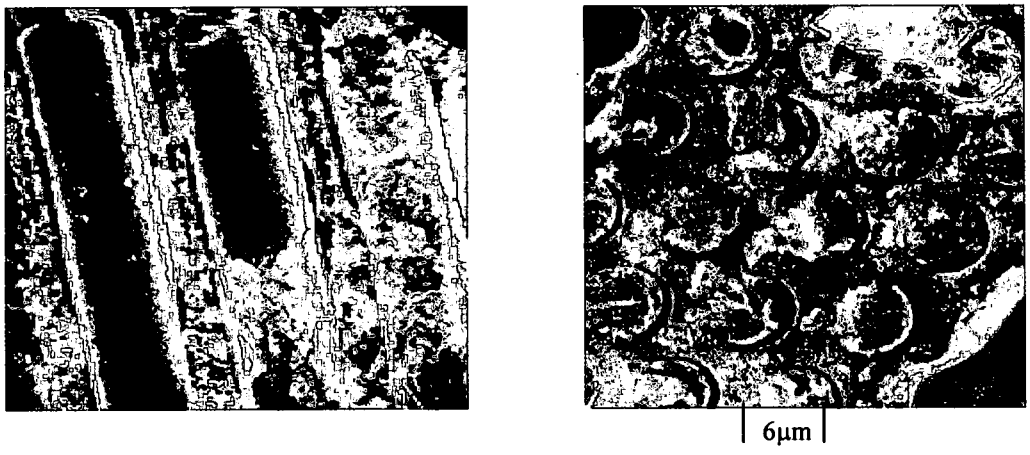

a b

Figure 4.3.2 SEM image of crystal growth of $Tb^{+3}GdCl_3$ inside 6 μm channel glass.

An electron diffraction image of $GdCl_3$ inside the 6 μm channels is shown in Figure 4.3.3. The image was taken within several channels and is indicative of single crystal structure.

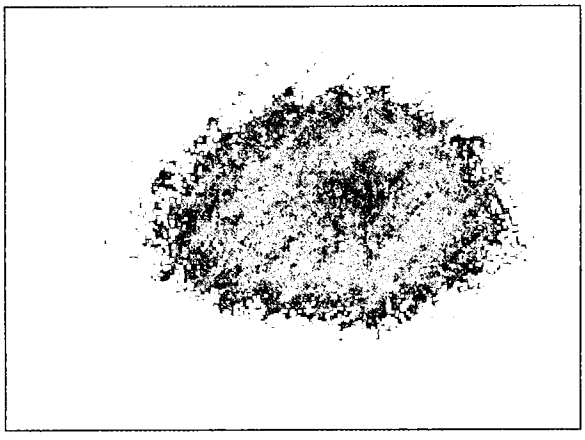

Figure 4.3.3 Electron diffraction of single crystal growth inside 6 μm channel.

Progress towards single crystal growth of $GdCl_3$ and Tb^{+3}:$GdCl_3$ has been accomplished inside of photonic crystals. It is apparent that it is indeed possible to wick the molten material into the channels of the photonic crystal and subsequently grow moderate domains of single crystals inside these channels. Unfortunately, initial growths are mixed single and polycrystalline domains within the channels.

Absorption spectra performed on the channel glass crystals show a λ^{-4} scattering profile which is indicative of large area polycrystaline structure. X-ray diffraction also produced results characteristic of the mixed domains of polycrystalline structures. Impurities, most often oxychlorides, in the crystal melt will inhibit single crystal growth. Each of the growths thus far have been tested

by placing portion of the crystal material in a 50ml and 1ml HCl solution. Any precipitate remaining after the crystal has dissolved is an impurity. Fortunately this has not been the cause for the polycrystalline growths. Self seeding is required and, in at least one case, has been the culprate for improper growth of the crystals. Crystals are grown under chlorine gas and its seems that a pocket of this gas became trapped at the tip of the ampoule and did not allow the melt to self seed as it cooled. To overcome this problem the ampoule is held under vacuum until just after the sample melts, at which time the ampoule is flooded with chlorine, other wise the molten sample will decompose in the vacuum. Refinement of the growth is a continuing process.

Thermal properties, most importantly differing thermal expansion coeficients and melting points, of the host materials and the photonic crystal materials have ihibited the growth of other species. Many of the host materials have high metlting points making them incompatable with the glasses of the photonic crystals presently in use. As seen in Figure 5b, differing thermal properties of the materials caused an expansion of the host crystal out of the nano-channel glass. Alternative low-phonon materials are being examined including gadalinium lanthinum sulfide (GLS) glass and KPb_2Cl_5 crystals. GLS glass and KPb_2Cl_5 readily incorporate the rare earth ions into their amorphous and crystaline structures respectively. Both of these materials have melting points well below the photonic crystal melt point, for example KPb_2Cl_5 recrystalizes around 430°C. Advantages include better thermal compatability with the photonic crystals and less stringent growth conditions.

CHAPTER 5

Conclusions and Future Work

In this thesis the methods for construction and the analysis of photonic crystal structures have been presented. The BPM approach, with some modification, will be a useful tool for examining the properties of these structures. I has been shown that photonic crystal structures can be fabricated almost instantaneously, through laser induced photopolymerization, therefore, formulating a real time analysis tool for this fabrication technique and the resulting structures is desirable. Holographic two-photon induced photopolymerization was successfully employed to produce one-dimensional photonic crystals with the periodicity ranging from 200 nm to 3 μm. In addition, incorporation of liquid crystal into one and two-dimensional photonic crystals was accomplished successfully in creating dynamic photonic structures and optical switches.

The analytical solution presented in this thesis is an approach that has been proven by experiment and is known to be accurate. The BPM code presented in this work is a first step toward numerically modeling these structures. It will be

necessary to combine the approaches to the one and two-dimensional structures, including reflections and scattering among other factors, to produce an accurate model. Dynamic systems will require a model such as this for the reason that it will be able to take into account the effects of linear and nonlinear optically active materials, defects, and other dynamics. This numerical solution could model the dynamics of a system fabricated using the presented holographic technique by modeling the system from the initial interference of the recording beams through the final structure. The model could take into account, among other parameters, phase separation, two-photon absorption, and other nonlinear effects in the material. The presented results show progress towards accomplishing a reasonable model for these materials.

Construction of one-dimensional photonic crystal structures via the holographic two-photon induced photopolymerization technique shows promise as a manufacturing method that can quickly and easily fabricate nano and micron scale devices. These structures have features on the scale of wavelengths of optical radiation, giving them the ability to control the propagation of light in this wavelength region. H-TPIP improves on the one-photon process by producing structures with reduced feature dimensions and higher definition as well as offering the ability to fabricate at depth in the material due to fact that there is no linear loss. This method also provides better control of the device features due to the fact that the process is intensity dependent as opposed to the fluence dependence of the one-photon process. Structures with dimensions smaller or larger than this can easily be fabricated, by adjusting the angle subtended by the

two beams and the magnitude of the intensity profile. Construction of a two-dimensional structure using H-TPIP is currently being investigated and it is expected that this will be successful by the publishing date of this thesis. Two-dimensional photonic crystals produced by NRL have features ranging from tens of nanometers to several microns. Crystals available to us did not show a large band gap, which, depending on the application, limits their use as stand alone photonic crystals. Doping semiconductor materials into the glass of the matrix material to increase the refractive index and reducing the spacing of the channels can increase the photonic band gap produced by these materials. Incorporation of other materials inside the channels can possibly enhance the band gap of the NCG as well.

Incorporating LC into the one-dimensional photonic crystal produced an optical switch or dynamic filter. Applying a voltage to the sample shifted the band gap and produced an on or off state for the wavelength falling inside the gap. This system could be used to modulate a beam in an optical communication system or to act as a dynamic notch filter. Filling the nano channel glass with LC also showed promise as an optical switch or multiplexing system. It would be of interest to design a similar system with a NCG sample of a slightly higher refractive index. Doing so could provide a situation where the ordinary refractive index of the liquid crystal will be less than the index of the glass matrix. This would offer the ability to switch between the waveguiding and inhibition of waveguiding by applying a field parallel or perpendicular to the channels. In addition, it is proposed that individual channels could be addressed, similar to

addressing micro-mirror arrays, in a multiplexing arrangement to provide high-speed communication links between multiple channels. It is also believed that intensity dependent filters can be constructed using a photonic crystal structure by incorporating a material with a large nonlinear index of refraction [16,61,62,63]. When the appropriate field is applied to the structure the index of the nonlinear material can be altered to produce a band gap for a particular wavelength. Incorporation of a nonlinear material exhibiting a thermal nonlinearity into the channels of a NCG sample has exhibited such dynamic behavior of the band gap of a two-dimensional photonic crystal [61,62,63].

Moderate success in the growth of single crystals of rare earth doped low phonon crystals inside the channels of the NCG was accomplished. Growth of these materials proved to be quite difficult and improvements on the growth apparatus must be made to facilitate better growths. Some improvements lie in a more exact understanding of the temperature gradient inside the furnace and knowledge of the exact position that melting occurs for a given sample. Melting points of several of the low phonon host candidates are incompatable with the glass of the NCG. Therefore, alternative low-phonon materials are being examined including gadalinium lanthinum sulfide (GLS) glass and KPb_2Cl_5 crystals. For example KPb_2Cl_5 recrystalizes around 430°C, well below the melting point of the NCG glass. These materials are more easily grown and readily incorporate the rare earth ions into their amorphous and crystaline structures respectively. These material offer better thermal compatability with the photonic crystals and less stringent growth conditions.

The above photonic crystal system show promise in the field of optical switching, filtering, and IR laser and detector technologies. Each system described is innovative and useful and will no doubt find a place in the field of optics. Photonic crystals are at the forefront of scientific discovery and will provide a source of scientific research for years to come.

APPENDIX A

MatLab Code for the Eigenvalue Solution and BPM

A1 Transverse Electric Eigenvalue Solution, translated from reference 68

```
clear all
%=================================================================
%                              Constants
%=================================================================

m=1;                          %meter
cm=0.01*m;                  %centimeter
mm=0.001*m;                 %milimeter
um=1*10^(-6)*m;             %micrometer
nm=1*10^(-9)*m;             %nanometer

s=1;                          %second
ms=0.001*s;                 %millisecond
us=1*10^(-6)*s;          %microsecond

c=3*10^8*m/s;                 %speed of light


d=0.72*um                   %channel Diameter
a=0.75*um                   %channel Spacing

nc=1                  %channel index
nb=3.6                     %glass index

epsa=nc^2                %channel dielectric
epsb=nb^2                %background dielectric(matrix dielectric)


G1x=2*pi;                   %Reciprocal Lattice Vectors
G1y=-2*pi/sqrt(3);          %Reciprocal Lattice Vectors

G2x=0;                             %Reciprocal Lattice Vectors
G2y=2*2*pi/sqrt(3);%Reciprocal Lattice Vectors

%=================================================================
%                    Wave Vectors
%=================================================================
```

```
'Building Wavevectors'
L=0;

for i=-9:1:9;
   for j=-9:1:9;

      if((i+j)>=-9)
            if ((i+j)<=9)
              L=L+1;
                 gx(L)= G1x*i + G2x*j;
                 gy(L)= G1y*i + G2y*j;
            end
      end
   end
end

k=1:L;                          %Index for use in latter sections

figure(1);
clf
hold on
plot(gx(k), gy(k),'.');
title('Wavevectors Inside the First Brillouin Zone')
'Done Building Wavevectors'

%=================================================================
%                  Dielectric Matrix
%=================================================================
'Constructing Dielectric Matrix'
beta = 2*pi*((d/2)^2/a^2)/sqrt(3)

for i=1:1:L;
    epsmatrix(i,i)= beta*epsa + (1-beta)*epsb;
end

for i=1:1:L;
   ii=i+1;
   for j=ii:1:L;
      x=gx(i)-gx(j);
         y=gy(i)-gy(j);
      Gr=sqrt(x^2+y^2)*d/2/a;                                    %Gr
for the bessel functions
         epsmatrix(i,j)= 2*beta*(epsa-epsb)*besselj(1,Gr)/Gr;

         epsmatrix(j,i)=epsmatrix(i,j);
   end
end

epsmatrix=inv(epsmatrix);

'Dielectric Matrix Complete'

%=================================================================
%                  Eigenvalue Calculation
%=================================================================
'Calculating Eigenvalues'
```

```
GxG=0;
GyG=0;
GxX=0;
GyX=2*pi/sqrt(3);
GxJ=2*pi/3;
GyJ=2*pi/sqrt(3);

gxi(1)=GxG;
gyi(1)=GyG;
gxi(2)=GxX;
gyi(2)=GyX;
gxi(3)=GxJ;
gyi(3)=GyJ;
gxi(4)=GxG;
gyi(4)=GyG;

index = 0;
for nk=1:1:3;
   nk1=nk+1;
   nmax=10;
   for jj=1:nmax

      index = index + 1;

      dkx=(jj-1)*(gxi(nk1)-gxi(nk))/nmax + gxi(nk);
      dky=(jj-1)*(gyi(nk1)-gyi(nk))/nmax + gyi(nk);

      for i=1:1:L
         aa(i,i)=epsmatrix(i,i)*((dkx+gx(i))^2                    +
(dky+gy(i))^2)/4/(pi^2);
         bb(i,i)=1;
         for j=i+1:1:L
            aa(i,j)=
epsmatrix(i,j)*((dkx+gx(i))*(dkx+gx(j))+(dky+gy(i))*(dky+gy(j)))/
4/(pi^2);
            aa(j,i)= aa(i,j);
            bb(i,j)= 0;
            bb(j,i)= 0;
         end
      end


      kvalues(index)=sqrt(dkx^2+dky^2);

      answers=eig(aa,bb);
      answers=sort(answers);
      answersb=answers;
      count=1;
      %for n=1:length(answers)
      %if sign(answers(n))==-1
      %else
      %answersb(count)=answers(n);
      %count=count+1;
      %end
      %end

      for pp=1:10;
```

```
         wavelength(index,pp)=2*pi/sqrt(answersb(pp));
         frequency(index,pp)=sqrt(answersb(pp));
         freqsqrd(index,pp)=answersb(pp);
      end
   end
end

'Eigenvalue Calculations Complete'
%frequency(1,1)=a;
%frequency(1,2)=d;
%frequency(1,3)=nc;
%frequency(1,4)=nb;

kvalues
frequency

figure(2)
clf
hold on
title('Band Structure for E-polarization (frequency)')

for mm=1:1:index
   for dd=1:1:pp
      plot(mm,frequency(mm,dd));
   end
end

%save d:\answers.dat answersb -ascii
save d:\hfyresults.dat frequency -ascii
```

A2 Transverse Magnetic Eigenvalue Solution, translated from reference 68

```
clear all
%=================================================================
%                              Constants
%=================================================================

m=1;                          %meter
cm=0.01*m;                 %centimeter
mm=0.001*m;                %milimeter
um=1*10^(-6)*m;            %micrometer
nm=1*10^(-9)*m;            %nanometer

s=1;                          %second
ms=0.001*s;                %millisecond
us=1*10^(-6)*s;         %microsecond

c=3*10^8*m/s;                 %speed of light


d=0.72*um                  %channel Diameter
```

```
a=0.75*um                %channel Spacing

nc=1                %channel index
nb=3.6                   %glass index

epsa=nc^2              %channel dielectric
epsb=nb^2              %background dielectric(matrix dielectric)


G1x=2*pi;                %Reciprocal Lattice Vectors
G1y=-2*pi/sqrt(3);       %Reciprocal Lattice Vectors

G2x=0;                           %Reciprocal Lattice Vectors
G2y=2*2*pi/sqrt(3);%Reciprocal Lattice Vectors

%=====================================================================
%                   Wave Vectors
%=====================================================================

'Building Wavevectors'
L=0;

for i=-9:1:9;
   for j=-9:1:9;

      if((i+j)>=-9)
            if ((i+j)<=9)
              L=L+1;
                 gx(L)= G1x*i + G2x*j;
                 gy(L)= G1y*i + G2y*j;
            end
      end
   end
end

k=1:L;                           %Index for use in latter sections

figure(1);
clf
hold on
plot(gx(k), gy(k),'.');
title('Wavevectors Inside the First Brillouin Zone')
'Done Building Wavevectors'

%=====================================================================
%                   Dielectric Matrix
%=====================================================================
'Constructing Dielectric Matrix'
beta = 2*pi*((d/2)^2/a^2)/sqrt(3)

for i=1:1:L;
    epsmatrix(i,i)= beta*epsa + (1-beta)*epsb;
end

for i=1:1:L;
   ii=i+1;
   for j=ii:1:L;
```

```
      x=gx(i)-gx(j);
         y=gy(i)-gy(j);
      Gr=sqrt(x^2+y^2)*d/2/a;                                        %Gr
for the bessel functions
         epsmatrix(i,j)= 2*beta*(epsa-epsb)*besselj(1,Gr)/Gr;

         epsmatrix(j,i)=epsmatrix(i,j);
   end
end

epsmatrix=inv(epsmatrix);

'Dielectric Matrix Complete'

%=================================================================
%                  Eigenvalue Calculation
%=================================================================
'Calculating Eigenvalues'
GxG=0;
GyG=0;
GxX=0;
GyX=2*pi/sqrt(3);
GxJ=2*pi/3;
GyJ=2*pi/sqrt(3);

gxi(1)=GxG;
gyi(1)=GyG;
gxi(2)=GxX;
gyi(2)=GyX;
gxi(3)=GxJ;
gyi(3)=GyJ;
gxi(4)=GxG;
gyi(4)=GyG;

index = 0;
for nk=1:1:3;
   nk1=nk+1;
   nmax=10;
   for jj=1:nmax

      index = index + 1;

      dkx=(jj-1)*(gxi(nk1)-gxi(nk))/nmax + gxi(nk);
      dky=(jj-1)*(gyi(nk1)-gyi(nk))/nmax + gyi(nk);

      for i=1:1:L
         aa(i,i)=epsmatrix(i,i)*((dkx+gx(i))^2                       +
(dky+gy(i))^2)/4/(pi^2);
         bb(i,i)=1;
         for j=i+1:1:L
            aa(i,j)=
epsmatrix(i,j)*((dkx+gx(i))*(dkx+gx(j))+(dky+gy(i))*(dky+gy(j)))/
4/(pi^2);
            aa(j,i)= aa(i,j);
            bb(i,j)= 0;
            bb(j,i)= 0;
         end
```

```
      end


      kvalues(index)=sqrt(dkx^2+dky^2);

      answers=eig(aa,bb);
      answers=sort(answers);
      answersb=answers;
      count=1;
      %for n=1:length(answers)
      %if sign(answers(n))==-1
      %else
      %answersb(count)=answers(n);
      %count=count+1;
      %end
      %end

      for pp=1:10;
         wavelength(index,pp)=2*pi/sqrt(answersb(pp));
         frequency(index,pp)=sqrt(answersb(pp));
         freqsqrd(index,pp)=answersb(pp);
      end
   end
end

'Eigenvalue Calculations Complete'
%frequency(1,1)=a;
%frequency(1,2)=d;
%frequency(1,3)=nc;
%frequency(1,4)=nb;

kvalues
frequency

figure(2)
clf
hold on
title('Band Structure for E-polarization (frequency)')

for mm=1:1:index
   for dd=1:1:pp
      plot(mm,frequency(mm,dd));
   end
end

%save d:\answers.dat answersb -ascii
save d:\hfyresults.dat frequency -ascii
```

A3 Beam Propagation for Two Dimensional Photonic Crystal

```
%Beam Propagation for Two Dimensional Photonic Crystal

clear all;
clc;

array=2^6                                          %array size
newarray=2^13

%Define Constants

cm=10^(-2);                                        %centimeter
multiplier
mm=10^(-3);                                        %milimeter
multiplier
um=10^(-6);                                        %micron
multiplier
nm=10^(-9);                                  %nanometer multiplier

ms=10^(-3);                                  %milisecond
us=10^(-6);                                  %microsecond
ns=10^(-9);                                  %nanosecond
ps=10^(-12);                                 %picosecond
fs=10^(-15);                                 %femtosecond

Hz=10^0;
kHz=10^3;

im=sqrt(-1);                                       %define i for
complex numbers

%Photonic Crystal Parameters

%*** It is important that the linear index n0m and n0c be
slightly different for condition later***

n0m = 1.6                  %Linear index of matrix material
n2m = 0.0          %Nonlinear index of matrix material

n0c = 1.0                        %Linear index of channel material
n2c = 0.0                        %Nonlinear    index    of    channel
material

channdia=300*nm;                  %Channel Diameter
spacing=450*nm;              %Channel spacing

%Set up input parameters for the field

wo=20*um                                           %beam   waist   at
entrance to crystal (focus)
eo=8.8542*10^(-12);                          %perm. of free space
c=3e10;                                %speed of light cm/s
Pw=1*10^(-3);                                %average      initial
pump power (Watts)
```

```
pulse=100*fs;                          %pulse width
rep=500*Hz;                            %repetition rate

Pwpulse = (Pw/rep/pulse);              %power per pulse

Intensity = Pwpulse/(pi*wo^2);         %Intensity (W/m^2)

Intensity = Intensity/((10^2)^2)    %convert Intensity to (W/cm^2)

Intensity = Intensity*10^7          %conver from MKS to esu

Ewo = sqrt(Intensity*2*pi/1/c)      %guassian field amplitude


%Define the Wavelength Range

startWL=10*nm;                          %Start Wavelength
endWL=1300*nm;                             %End Wavelength
step=5*nm;                             %Wavelength Step Size

lambdarray=startWL:step:endWL-step;

%================================================================
%This function builds the propagation cells for the BPM loop
%================================================================

xwindow=spacing;                              %length of the NxM array
[m]
zwindow=spacing*sqrt(3)/2;                     %width of the NxM array
[m]
dx=xwindow/array;                              %dx   distance   between
pixels [m/pixel]
dz=zwindow/array;                                %dz step size through
crystal



%----------------------------------------------------------------
%Unit Cell Array for Cylindrical Channel
%----------------------------------------------------------------

%Generate an array containing the values of x^2+y^2 for the
channel

length=-xwindow/2:dx:xwindow/2-dx;
width=-zwindow/2:dz:zwindow/2-dz;
[x1,y1]=meshgrid(length,width);

%Unit Cell Arrays for Circular Channel

unitcell=zeros(array,array);                   %open an NxN array for
the aperture
R=sqrt(x1.^2+y1.^2);                           %calculate   the   x/y
radius
```

```
for i=1:array;                                    %x   deminsion   of
unitcell
   for j=1:array;                                 %y   deminsion   of
unitcell
      if R(i,j)<=channdia/2;          %Define the channel indices
         unitcell1(i,j)=1;          %define channel index
      else
         unitcell1(i,j)=2;         %define matrix
      end%if loop
   end%j loop
end%i loop


%build unit cell for second row
for i=1:array/2;
   unitcell2(i,:)=unitcell1(i+array/2,:);
   unitcell2(i+array/2,:)=unitcell1(i,:);
end

%-----------------------------------------------
%Build Main Cells
%-----------------------------------------------
%numcells=round((wo*20)/xwindow);                 %Number of cells
to fit 20*wo
%newarray=numcells*array;                          %Everything is
based on this array size

cellength=(newarray)*dx                          %Cell length in [m]

cellwindow=-cellength/2:dx:cellength/2-dx;       %New   window   to
propagate through
cellwindow=cellwindow';



cell1=zeros(newarray,array);
cell2=zeros(newarray,array);
NLcell1=zeros(newarray,array);
NLcell2=zeros(newarray,array);


cellind=1;
while cellind<=(newarray)
   for ii=1:array
      cell1(cellind,:)=unitcell1(ii,:);
      cell2(cellind,:)=unitcell2(ii,:);
      NLcell1(cellind,:)=unitcell1(ii,:);
      NLcell2(cellind,:)=unitcell2(ii,:);
      cellind=cellind+1;
   end
end

%================================================================
%BPM BPM BPM BPM BPM BPM BPM BPM BPM BPM BPM BPM BPM BPM BPM
BPM BPM BPM BPM BPM BPM
%================================================================
```

```
%-------------------------------------------------
%Vince Stuff
%-------------------------------------------------

p=0:1:newarray-1;
ind=(min(p,(newarray-p)))';

%-------------------------------------------------
%BPM Loop
%-------------------------------------------------

%Open an Array for the Data


Data=zeros(abs(endWL-startWL)/step,10);              %Data Array
Data1=zeros(abs(endWL-startWL)/step,1);             %Data Array
Data2=zeros(abs(endWL-startWL)/step,1);             %Data Array



z=0.000000000001;                                    %Initialize
the z position
ll = 1;
count=3
%for count = 2:2:4                                          %Steps
through different prop lengths
   for jj=1:abs(endWL-startWL)/step;

      lambda=lambdarray(1,jj)
%wavelength
      ko=2*pi/lambda;
%wavevector
      zo=pi*wo^2/lambda
%Rayleigh range (m)
      wz=wo*sqrt(1+(z/zo)^2);
%beam waist at z
      rz=z*(1+(zo/z)^2);
%radius of curvature

      radprop=exp(-im*ko*pi*(cellwindow.^2)/(2*rz));
%radial phase
      Field=Ewo*exp(-(cellwindow.^2)/wz^2)*1/sqrt(1+(z/zo)^2);
%pump field
      Field1=Field.*radprop;
%amplitude and phase
      Field2=Field.*radprop;
%amplitude and phase field 2
      inField=Field.*radprop;
%amplitude and phase


      %figure(1)
      %clf;
      %
      for                                          iterate=1:count;
%2*number of propagation cells
         for m=1:array;
```

```
            I = n0m*c*(Field1.*conj(Field1))./2/pi;

            for pp = 1:newarray
               if cell1(pp,m) == 2
                  NLcell1(pp,m) = n0m + n2m*I(pp);
               else
                  NLcell1(pp,m) = n0c + n2c*I(pp);
               end
            end  %newarray

            PropPhase(:,1)=dz*pi*lambda.*ind.^2./((n0m          +
n2m*I(1:newarray)).*cellength^2);
            Field1=ifft(fft(Field1).*exp(-im*PropPhase));
%Propagation

            ModPhase(:,1)=2*pi.*NLcell1(:,m).*dz/lambda;
            Field1=Field1.*exp(im.*ModPhase);
%Modulation


            PropPhase2(:,1)=dz*pi*lambda.*ind.^2./((n0m          +
n2m*I(1:newarray)).*cellength^2);          %Propagation  through
homogenous mat
            Field2=ifft(fft(Field2).*exp(-im*PropPhase2));
%No modulation
            Field2=Field2;

         end  %array


         for m=1:array;

            I = n0m*c*(Field1.*conj(Field1))./2/pi;

            for pp = 1:newarray
               if cell2(pp,m) == 2
                  NLcell2(pp,m) = n0m + n2m*I(pp);
               else
                  NLcell2(pp,m) = n0c + n2c*I(pp);
               end
            end

            PropPhase(:,1)=dz*pi*lambda.*ind.^2./((n0m          +
n2m*I(1:newarray)).*cellength^2);
            Field1=ifft(fft(Field1).*exp(-im*PropPhase));
%Propagation
            ModPhase(:,1)=2*pi.*NLcell2(:,m).*dz/lambda;
            Field1=Field1.*exp(im.*ModPhase);
%Modulation

            PropPhase2(:,1)=dz*pi*lambda.*ind.^2./((n0m          +
n2m*I(1:newarray)).*cellength^2);          %Propagation  through
homogenous mat
            Field2=ifft(fft(Field2).*exp(-im*PropPhase2));
%No modulation
            Field2=Field2;
```

```
        end  %array
      end  %iterate
      %====================================
      %Propagate to the detector
      %====================================
      PropPhase(:,1)=1000*dz*pi*lambda.*ind.^2./(1*cellength^2);
      Field1=ifft(fft(Field1).*exp(-im*PropPhase));
%Propagation

      PropPhase2(:,1)=1000*dz*pi*lambda.*ind.^2./(1*cellength^2);
%Propagation through homogenous mat
      Field2=ifft(fft(Field2).*exp(-im*PropPhase2));

      sum1=0;
%sum will be the integration of the field
      sum2=0;
      for oo=round(newarray/4):round(3*newarray/4)
         sum1=sum1+(Field1(oo).*conj(Field1(oo)));
         sum2=sum2+(Field2(oo).*conj(Field2(oo)));
      end

      Data1(jj,1)= sum1;
      Data2(jj,1)= sum2;
   end
   propdistance=2*iterate*spacing
   sum1=sum1
   sum2=sum2


   pp=1:jj;

   Data(pp,ll)=Data1(pp,1)./Data2(pp,1);

   figure(8);
   clf
   hold on;
   plot(lambdarray(1,pp),Data(pp),'-');
   title('Normalized Intensity');
   xlabel('Wavelength');
   ylabel('Normalized Intensity');
   ll = ll + 1;
%end  %count

save a:\transmit.dat Data -ascii
```

A4 Beam Propagation for One Dimensional Photonic Crystal

```
%Beam Propagation for One Dimensional Photonic Crystal at normal
incidence TE

clear all;
clc;

array=1                                          %array sze
newarray=2^2
```

```
%Define Constants

m=10^(0);                                   %meter multiplier
cm=10^(-2);                                         %centimeter
multiplier
mm=10^(-3);                                         %milimeter
multiplier
um=10^(-6);                                         %micron
multiplier
nm=10^(-9);                                 %nanometer multiplier

ms=10^(-3);                                 %milisecond
us=10^(-6);                                 %microsecond
ns=10^(-9);                                 %nanosecond
ps=10^(-12);                                %picosecond
fs=10^(-15);                                %femtosecond

Hz=10^0;
kHz=10^3;

im=sqrt(-1);                                        %define  i  for
complex numbers

%Photonic Crystal Parameters

%*** It is important that the linear index n0m and n0c be
slightly different for condition later***

n1 = 1.53                                     %Linear index of region 1
n2 = 1.535                                  %Linear index of region 2
n0 = 1.0                                    %Linear index of air

d1=120*nm                                     %length of region 1
d2=120*nm                                   %length of region 2
a=d1+d2                                     %periodicity

%losspm=0.05/m


tt=50
numlayers=2*tt                               %number of layers must be a
factor of two
num=numlayers/2;
n=zeros(1,numlayers+1);
for nn=0:num
   n(2*nn+1)=n1;
   n(2*nn+2)=n2;
   dz(2*nn+1)=d1/array;
   dz(2*nn+2)=d2/array;
end
n(numlayers+1)=1;
'index profile'
n
dz
wo=10*um
cellwidth=20*wo              %Cell length in [m]
dx=cellwidth/newarray
```

```
dz1=d1/array                    %dz step size through crystal for
region 1\
dz2=d2/array



%Define the Wavelength Range

startWL=700*nm;                          %Start Wavelength
endWL=820*nm;                            %End Wavelength
step=1*nm;                             %Wavelength Step Size

lambdarray=startWL:step:endWL-step;

%Define the input field
Ewo=1;

theta_i=0;
theta_t=asin(n1*sin(theta_i)/n2)

betas1=(n2*cos(theta_t))/(n1*cos(theta_i))
betas2=(n1*cos(theta_t))/(n2*cos(theta_i))
betas01=n1/n0;
betas02=n0/n1;

ts1=2/(1+betas1)
ts2=2/(1+betas2)
ts01=2/(1+betas01)
ts02=2/(1+betas02)

rs1=[n1*cos(theta_i)-
n2*cos(theta_t)]/[n2*cos(theta_t)+n1*cos(theta_i)];
rs2=[n2*cos(theta_i)-
n1*cos(theta_t)]/[n1*cos(theta_t)+n2*cos(theta_i)];

rs1=abs(rs1)
rs2=abs(rs2)
ts1=1-rs1;
ts2=1-rs2;

%================================================================
%This function builds the propagation cells for the BPM loop
%================================================================

%Each region may have different depths so it is neccesary to set
up two cells of equal
%matrix elements with different step sizes relative to the region
size


cellwindow=-cellwidth/2:dx:cellwidth/2-dx;       %New window to
propagate through
cellwindow=cellwindow';

%================================================================
%BPM BPM BPM BPM BPM BPM BPM BPM BPM BPM BPM BPM BPM BPM BPM BPM
%BPM BPM BPM BPM BPM BPM
```

```
%================================================================

%-------------------------------------------------
%Vince Stuff
%-------------------------------------------------

p=0:1:newarray-1;
ind=(min(p,(newarray-p)))';



%-------------------------------------------------
%BPM Loop
%-------------------------------------------------


z=0.0;                                          %Initialize the z
position
%ll = 1;
for jj=1:abs(endWL-startWL)/step;

   lambda=lambdarray(1,jj)                      %wavelength
   ko=2*pi/lambda;                              %wavevector
   Field=exp(-im*z*2*pi/lambda);                %input field
   inField=Field;                               %input field
   Fields=0;
   layer=0;
   for nn=0:numlayers-1;
      Field = inField;
      layer=layer+1;
      rs=[n(layer)*cos(theta_i)-
n(layer+1)*cos(theta_t)]/[n(layer+1)*cos(theta_t)+n(layer)*cos(th
eta_i)];
      if sign(rs)< 0
         Field=Field*exp(-im*pi);
      end
      rs=abs(rs);
      for m=1:layer;
         for zz=1:array;
            Field=Field*exp(-im*dz(m)*2*pi*n(m)/lambda);
            %Field=Field*(1-losspm*dz(m));
            %'forward'
            %n(m)
         end
      end
      for m=layer:-1:1
         for zz=1:array;
            Field=Field*exp(-im*dz(m)*2*pi*n(m)/lambda);
            %Field=Field*(1-losspm*dz(m));
            %'back'
            %n(m)
         end
      end
      %Field=ts01*ts02*rs*((ts1*ts2)^nn)*((rs1*rs2)^nn)*Field;
      Field=rs*((ts1*ts2)^nn)*Field;
      %Field=rs*Field;
      Fields=Fields + Field;
```

```
    end
    Fields;
    Fields*conj(Fields);

    answers(jj,1)=lambda;
    answers(jj,2)=a/lambda;
    answers(jj,3)=Fields*conj(Fields);
    answers(jj,4)=[(inField*conj(inField))-(Fields*conj(Fields))];

end
figure(1)
%clf;
hold on;
plot(answers(1:jj,2),answers(1:jj,4))


figure(2)
%clf;
hold on;
plot(answers(1:jj,1),answers(1:jj,4))



save d:\onedbpm.dat answers -ascii
```

REFERENCES

[1] J. D. Joannapoulos, R D. Meade, J N. Winn, *"Photonic Crystals: Molding the Flow of Light"*, Princeton University Press, New Jersey, 1995. et. al.

[2] E. Yablonovitch, *Inhibited Spontaneous Emission in Solid State Physics and Electronics*, Phys. Rev. Lett. 58(20), 2059, (1987).

[3] J.P. Dowling and C.M. Bowden, *Atomic emission rates in inhomogeneous media with applications to photonic band structures*, Phys. Rev. A. 46(1), 612, (1992).

[4] R. D. Meade, A.M. Rappe, K.D. Brommer, and J. D. *Joannopoulos, Accurate theoretical analysis of photonic band-gap materials*, Phys. Rev. B. 48, 8434, (1993) et. al.

[5] K.M. Leung and Y.F. Liu, *Full Vector Wave Calculation of Photonic Band Structure in Face-Centered-Cubic Dielectric Media*, Phys. Rev. Lett. 65, 2646, (1990)

[6] Ze Zhang and Sasi Satpathy, *Electromagnetic Wave Propagation in Periodic Structures: Bloch Wave Solution of Maxwell's Equations*, Phys. Rev. Lett. 65, 2650 (1990)

[7] K. M. Ho, C. T. Chan, and C. M. Soukoulis, *Existence of Photonic Gap in Periodic Dielectric Structures*, Phys. Rev. Lett. 65, 3152, (1990)

[8] J. W. Haus *Photonic Band Structures,* Quantum Optics of Confined Systems, eds. M. Ducloy and D. Bloch, Kluwer, Dordrecht, (1996)

[9] R. D. Meade, K.D. Brommer, A.M. Rappe, and J. D. Joannopoulos, *Existence of a photonic band gap in two dimensions*, Appl. Phys. Lett. 61(4), 495, (1992).

[10] R. D. Meade, K.D. Brommer, A.M. Rappe, and J. D. Joannopoulos, *Photonic bound states in periodic dielectric materials*, Phys. Rev. B 44(24), 13772, (1991).

[11] R.D. Meade, A.M. Rappe, K.D. Brommer, and J. D. Joannopoulos, *Nature of the photonic band gap: Some insights from a field analysis*, J. Opt. Soc. Am. B, 10(2), 328, (1993)

[12] E. Yablonovitch and J.J. Gmitter, *Photonic Band Structure: The Face-Centered-Cubic Case*, Phys. Rev. Lett. 46(1), 1950, (1989).

[13] H. S. Sozuer and J. W. Haus, *Photonic Bands: Converegence problems with the plane wave method*, Phys. Rev. B. 45(24), 13962, (1992).

[14] S. L. McCall and P. M. Platzman, *Microwave Propagation in Two-Dimensional Dielectric Lattices*, Phys. Review Lett. 67(15), 2017, (1991).

[15] S.John, *Strong Localization of Photons in Certain disordered Dielectric Superlattices,* Phys. Rev. Lett. 58(23), 2486, (1987).

[16] M. Scalora, J. P. Dowling, C.M. Bowden, M.J. Bloemer, *Optical Limiting and Switching of Ultrashort Pulses in Nonlinear Photonic Band Gap Materials*, Phys. Rev. Lett. 73, 1368-1371, (1994).

[17] J. W. Haus, private communication

[18] C. Kittel, "Introduction to Solid State Physics" 6th ed. John Wiley & Sons, Inc. New York, 1986.

[19] V. Dominic, *The Beam Propagation Method (BPM): A Tutorial*,Center for Electro-Optics, University of Dayton.

[20] C.R. Pollock, "Fundamentals of Optoelectronics", Richard D. Irwin Inc, Chicago, 1995.

[21] J.W. Goodman, "Inroduction to Fourier Optics" McGraw-Hill, NewYork, 1996.

[22] J. Van Roey, J. van der Donk, and P. E. Lagasse, *Beam propagation method: analysis and assessment*, , J. Opt. Soc. Am. 71(7), 803, (1981).

[23] D. Yevick, *Efficient Beam Propagation Techniques*, IEEE J. Quantum Elec. 26(1) 109, (1990).

[24] P.S. Weitzman, U. Osterberg, V. Dominic, *A Time-Dependent Beam-Propagation Method to Model Photoinduced Effects in Glass*, IEEE Journal of Quantum Electronics 30, 2970 (1994).

[25] M.D. Feit and J.A. Fleck, Jr. *Light propagation in graded index optical fibers,* Appl. Optics 17, 3990 (1978)

[26] R.V. Johnson and Armand R. Tanquay, Jr. *Optical beam propagation method for birefringent phase grating diffraction*, Optical Engineering 25, 235 (1986)

[27] D. Yevick and L. Thylen, *Analyisis of gratings by the beam propagation method*, J. Opt. Soc. Am. 72(8), 1084, (1982).

[28]J. A. Fleck, Jr., and M. D. Feit, *Beam propagation in uniaxial anisotropic media*, J. Opt. Soc. Am. 73(7), 920, (1983).

[29] P.S. Witzman and U. Osterberg, *A Modified Beam Propagation Method to Model Second Harmonic Generation In Optical Fibers*, IEEE J. Quantum Elec. 29(5), 1437, (1993).

[30] Optical Radiation and Matter, The University of Dayton Electro-Optics Program

[31] S.M. Kirkpatrick, J.W. Baur, C.M.Clark, L.R. Denny, D.W. Tomlin, B.R. Reinhardt, R. Kannan, M.O. Stone, *Holographic recording using two-photon-induced photopolymerization*, Appl. Phys. A 69, 461-464 (1999).

[32] R.A, Borisov, G.N. Dorojkina, N.I. Koroteev, V.M. Kozenkov, S.A. Magnitskii, D.V. Malakhov, A.V Tarasishin, A.M. Zheltikov, *Femtosecond two-photon photopolymerization: a method to fabricate optical photonic crystals with controllable parameters*, Laser Phys. 8(5), 1105-1108, (1998).

[33] S. Shoji and S. Kawata, *Photofabrication of three-dimensional photonic crystals by multibeam laser interference into a photopolymerizable resin,* American Institue of Physics 76(19), 2668 (2000)

[34] T.J. Bunning, S.M. Kirkpatrick, L.V. Natarajan, V.P. Tondiglia, D.W. Tomlin, *Electrically Switchable Gratings Formed Using Ultrafast Holographic Two-Photon Induced Photopolymerization (H-TPIP)*, AFRL MLPJ (2000)

[35] S. Maruo, O. Jakamura, and S. Kawata, *Three-dimensional microfabrication with two-photon-absorbed photopolymerization*, Optics Letters 22(2) 132 (1997).

[36] S. Kawakami, T. Kawashima, and T. Sato, *Mechanism of shape formation of three-dimensional periodic nanostructure by bias sputtering,* Appl. Phys. Lett. 74(3) 463 (1999).

[37] S. Shoji and S. Kawata, *Optically-induced growth of fiber patterns into a photoolymerizable resin*

[38] Norland Chemical Company: private communication

[39] J. T. Verdeyen, Laser Electronics, 3rd ed., Prentice Hall, Englewood Cliffs, New Jersey, 1995.

[40] Born and Wolf, "Principles of Optics" Cambridge University Press, New York, 1999

[41] T. Bunning, private communication

[42] R.J. Tonicci, B.L Justus, A.J. Campillo, C.E Ford, *Nanochannel Array Glass*, Science 258, 783-785, (1992).

[43] R. Tonicci: private communication

[44] D.H. Pearson and R.J. Tonucci, *Parallel Patterning with Nanochannel Glass Replica Membranes*, Adv. Mater. 8(12), 1031 (1996).

[45] Khoo, Iam-Choon, Wu, Shin-Tson, *Optics and Nonlinear Optics of Liquid Crystals*. Singapore, World Scientific, 1993.

[46] S. Elston, R. Sambles, ed., *The Optics of Thermotropic Liquid Crystals*, Taylor & Francis Ltd, London, 1998.

[47] R.Tonucci, personal communication

[48] T. Bunning, personal communication

[49] S.M. Kikpatrick, L.B. Shaw, S.R. Bowman, S. Searles, B.J. feldman, and Joseph Ganem, *Mid-Infrared Spectroscopy of Erbium Doped Chloride Laser Crystals,*OSA Optics Express 1, 78-86 (1997).

[50] S.M. Kirkpatrick, S. R. Bowman, L. B. Shaw, and S. Searles, *Investigation of a mid infrared erbium laser*,

[50] S. R. Bowman, L. B. Shaw, S. Searles, and B. J. Feldman, *Investigation of a potential mid-infrared erbium laser*, OSA TOPS Advanced Solid State Lasers (1998)

[52] S.R. Bowman, J. Ganem, B.J. Feldman, and A.W. Kueny, *Infrared laser characteristics of praseodymium-doped lanthanum trichloride,* IEEE J. Quantum Electronics. 30, 2925-2928, (1994).

[53] S.R. Bowman, L.B. Shaw, B.J. Feldman, and J. Ganem, *A 7 Micron Praseodymium-Based Solid State Laer,* IEEE J. Quantum Electron.,32, 646-649 (1996).

R00258728

[54] S.M. Kirkpatrick, S.R. Bowman, L.B. Shaw and Joseph Ganem, *Cross Relaxation and Upconversion Coefficients of Mid-IR of Pr^{+3}:$LaCl_3$*, J. Appl. Phys.,82 , pp. 2759-2765 (1997).

[55] J. P. Dowling, M.Scalora, M.J. Bloemer, and C.M. Bowden, *The photonic band edge laser: A new approach to gain enhancment*, J. Appl. Phys. 75(4), 1896 (1994).

[56] D. Kleppner, *Inhibited Spontaneous Emission*, Phys. Rev. Lett. 47(4), 233, (1981).

[57] B.R. Judd, *Optical Absorption Intensities of Rare-Earth Ions*, Phys. Rev. 127(3), 750, (1962).

[58] G.S. Ofelt, *Intenisities of Crystal Spectra of Rare-Earth Ions*, J. Chem. Phys. 37(3), 511, (1962).

[59] D.E. Cox and F.K. Fong, *Growth of Single Crystals of Anhydrous Lanthatnide Halides*, Journal of Crystal Growth.,20, pp. 233-238 (1973)

[60] C.M. Clark, S.M. Kirkpatrick, R.J. Tonucci, *Two Dimensional Photonic Band Gap Hosts for Rare Earth Doped Low Phonon Laser Crystal*, Unpublished, (1999).

[61] H-B. Lin, R. J. Tonucci, and A. J. Campillo, *Two-Dimensional Photonic Bandgap Optical Limiter in the Visible,* OCIS 1997

[62] R.W Boyd, "Nonlinear Optics", Academic Press, San Diego, 1992.

[63] R.A. Sutherland, "Handbook of Nonlinear Optics", Marcel Dekker, Inc.,New York, 1996.